



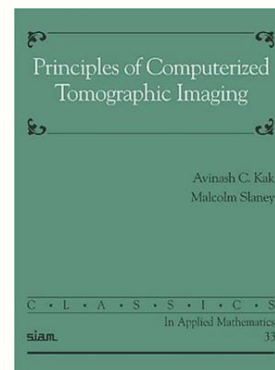
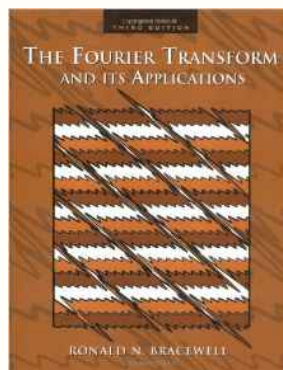
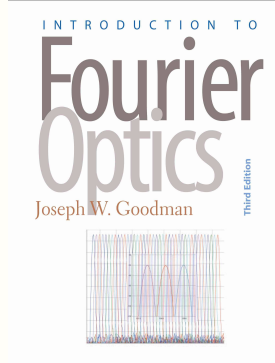
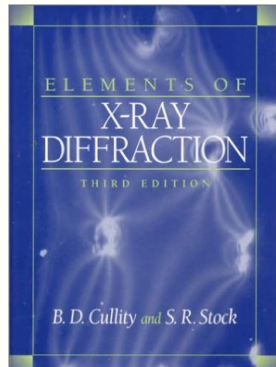
HERCULES 2022: Tutorial PXCT data analysis: phase retrieval and tomographic reconstruction

Julio Cesar da Silva

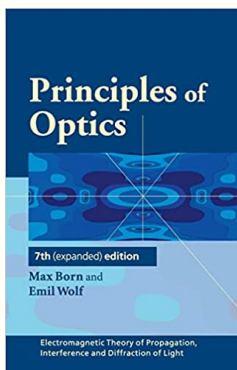
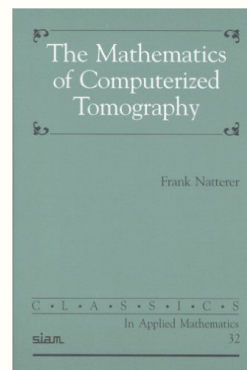
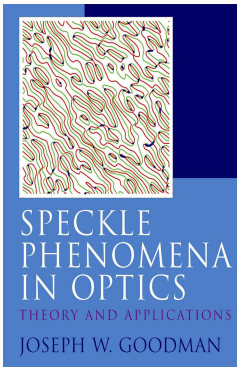
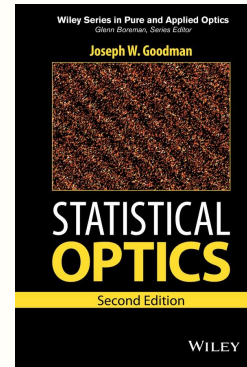
*Institut Néel CNRS/UGA & F-CRG beamlines, ESRF
Grenoble, France*

e-mail: julio-cesar.da-silva@neel.cnrs.fr

Fundamental ones:



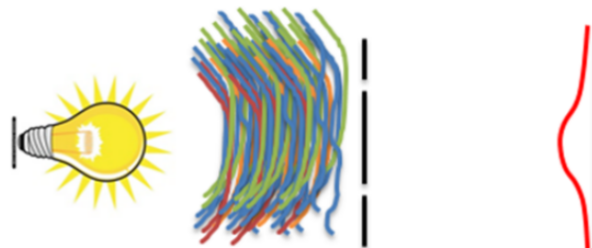
Also important ones:



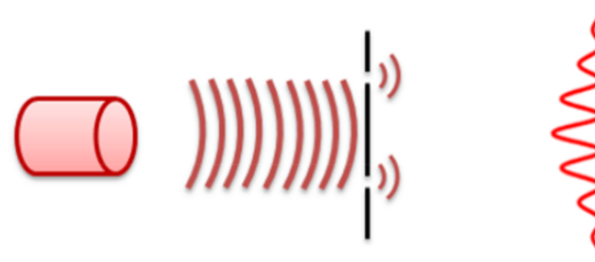
What is light?



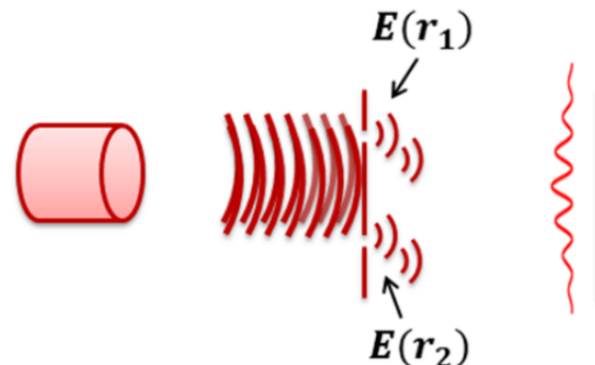
Complete
incoherence:



Complete
coherence:

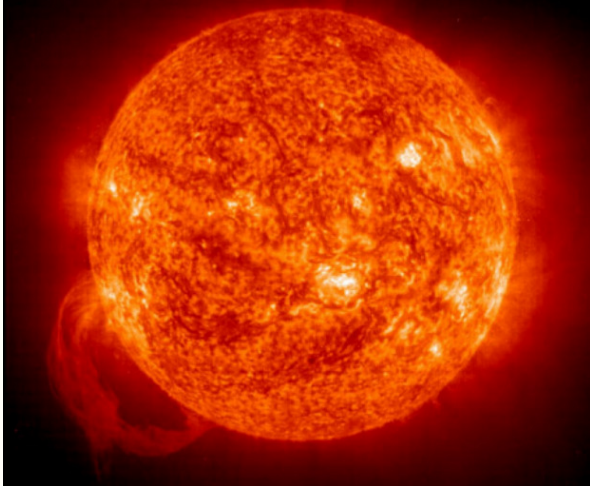


Partial
coherence:



Is the sunlight coherent?

<https://www.nationalgeographic.com/science/photos/sun-gallery/>



Double slit experiments



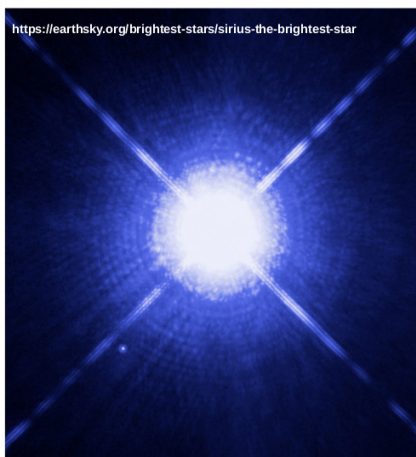
<https://www.youtube.com/watch?v=luv6hY6zsd0>

$$\text{Coherent Area } (A_c) \sim 4 \times 10^{-3} \text{ mm}^2$$

S. Divitt and L. Novotny, Optica 2(2), 95-103 (2015)

<https://skullsinthestars.com/2010/06/12/you-could-learn-a-lot-from-a-ducky-the-van-cittert-zernike-theorem/>

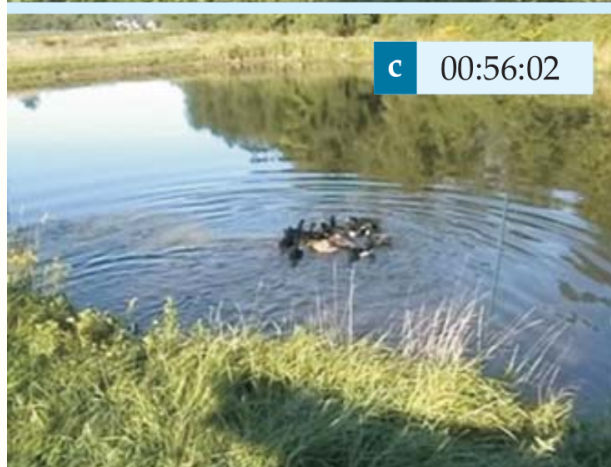
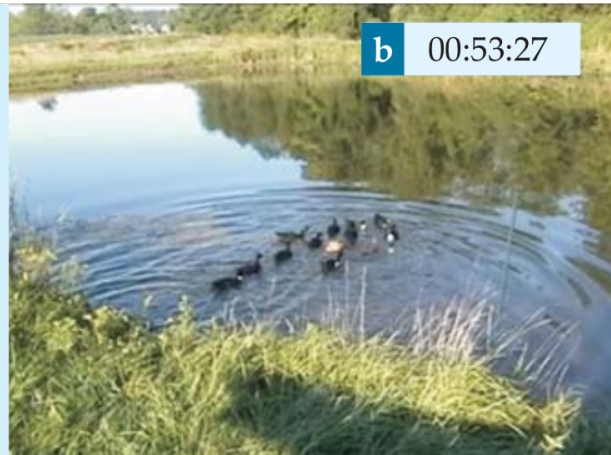
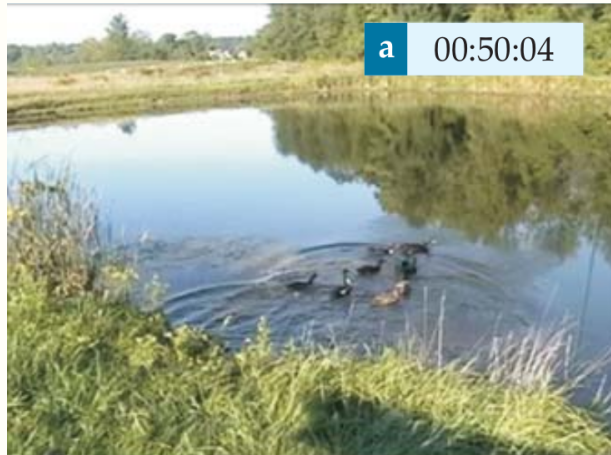
The light of a star



Coherent Area (A_c) $\sim 6 \text{ m}^2$

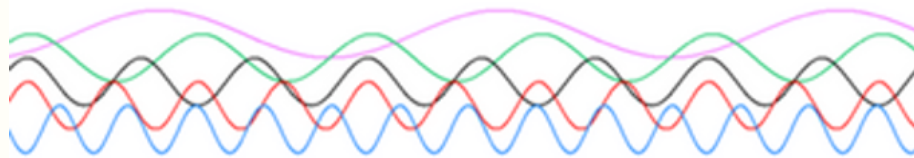
<https://skullsinthestars.com/2010/06/12/you-could-learn-a-lot-from-a-ducky-the-van-cittert-zernike-theorem/>

The van Cittert-Zernike theorem



<https://youtu.be/4o48J4streE>

Incoherent waves with different frequencies (and not monochromatic)

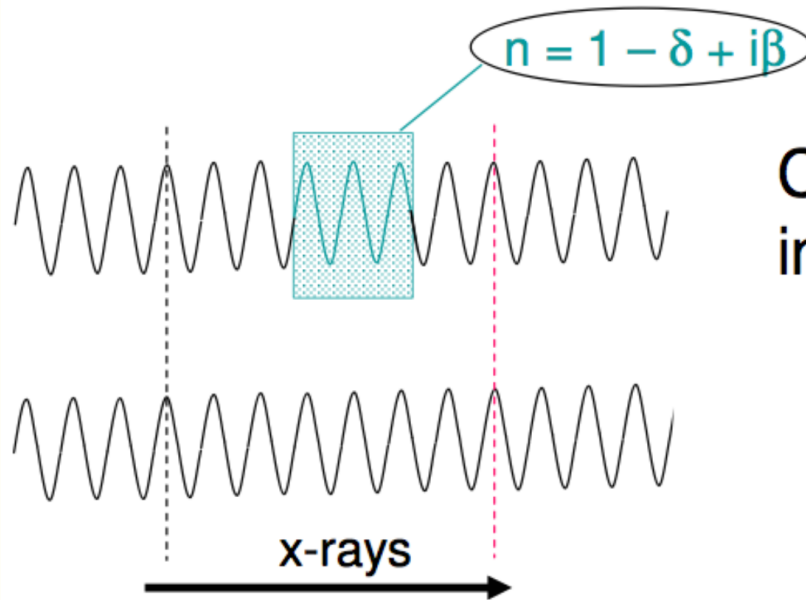


Incoherent waves with same frequency (and monochromatic)



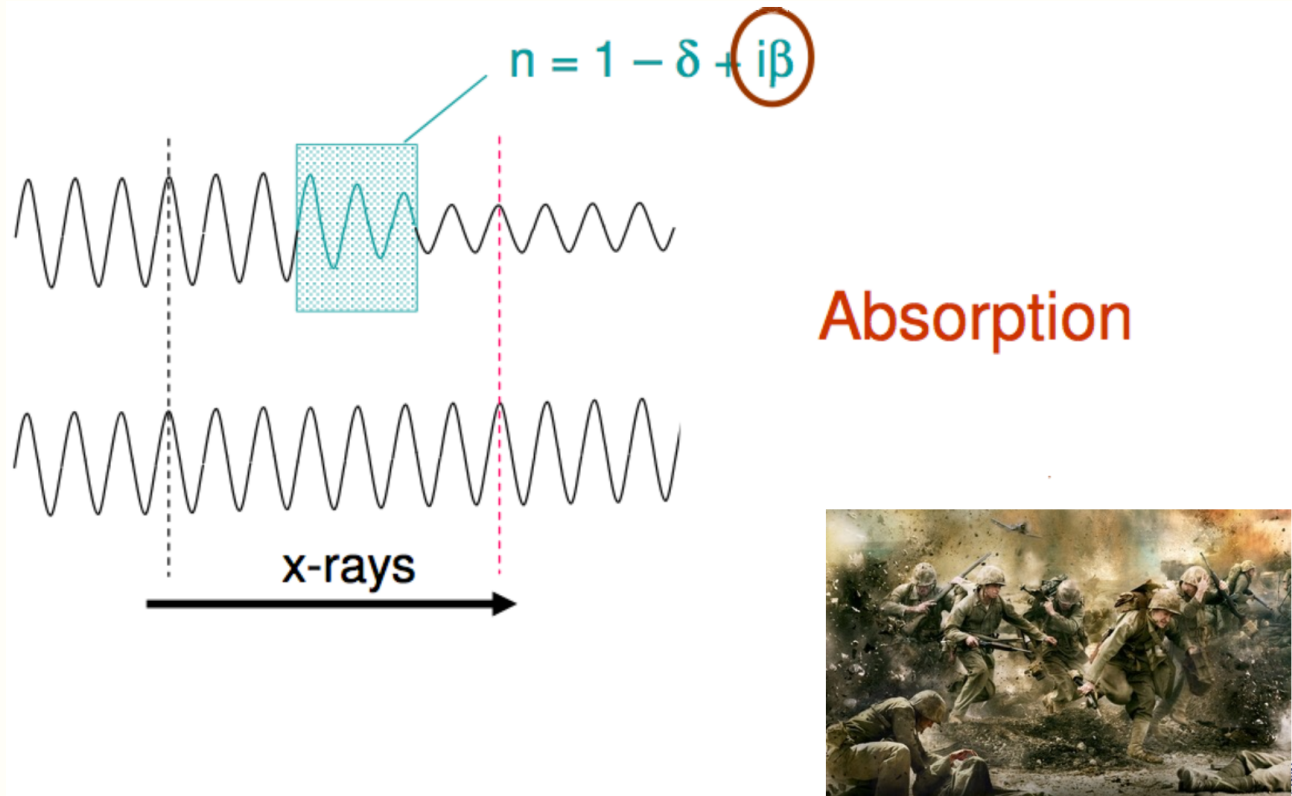
Coherent waves (and monochromatic)

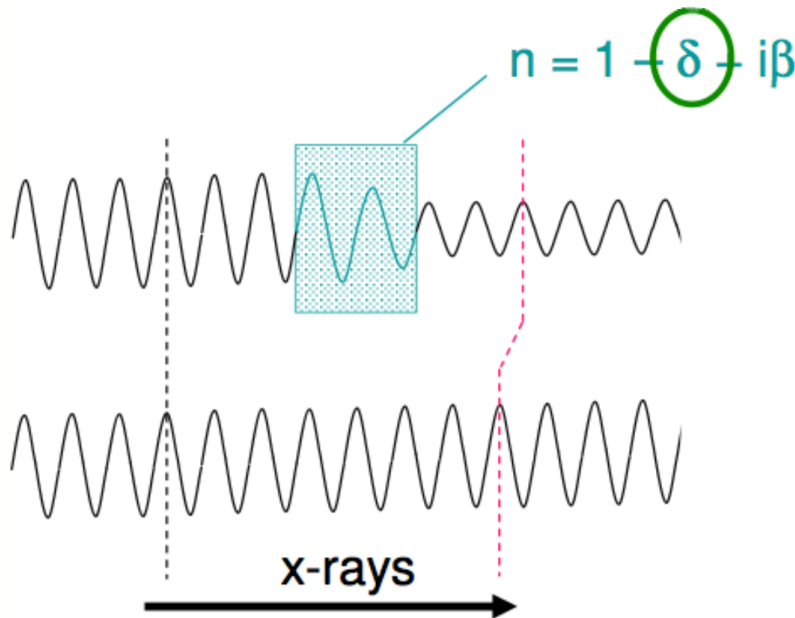




Complex-valued
index of refraction

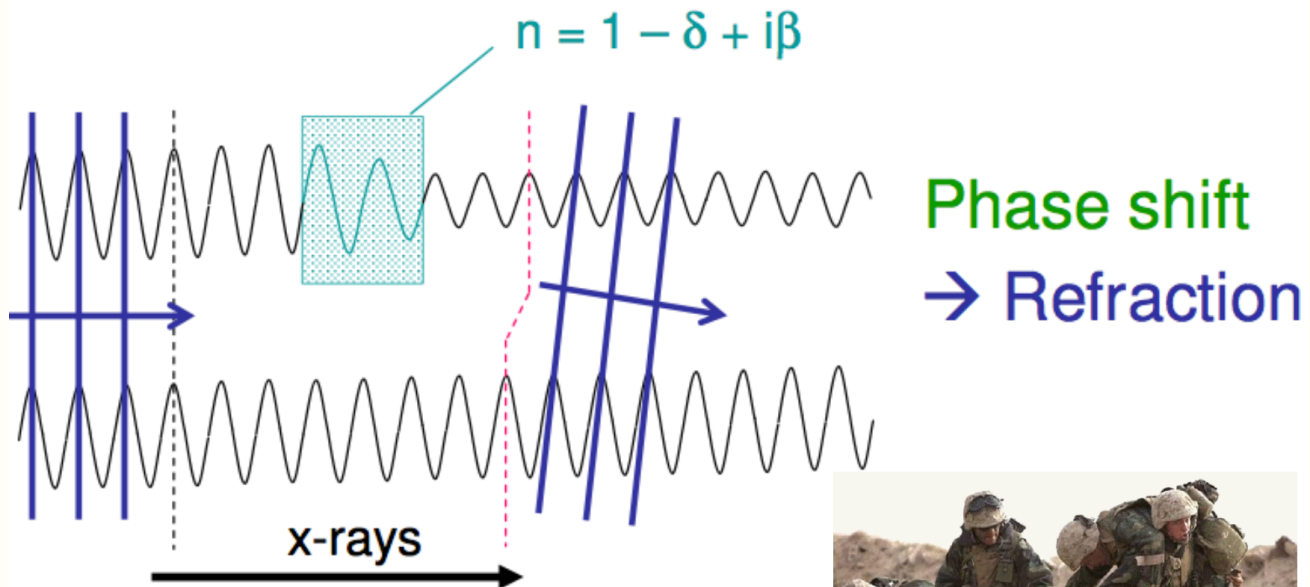




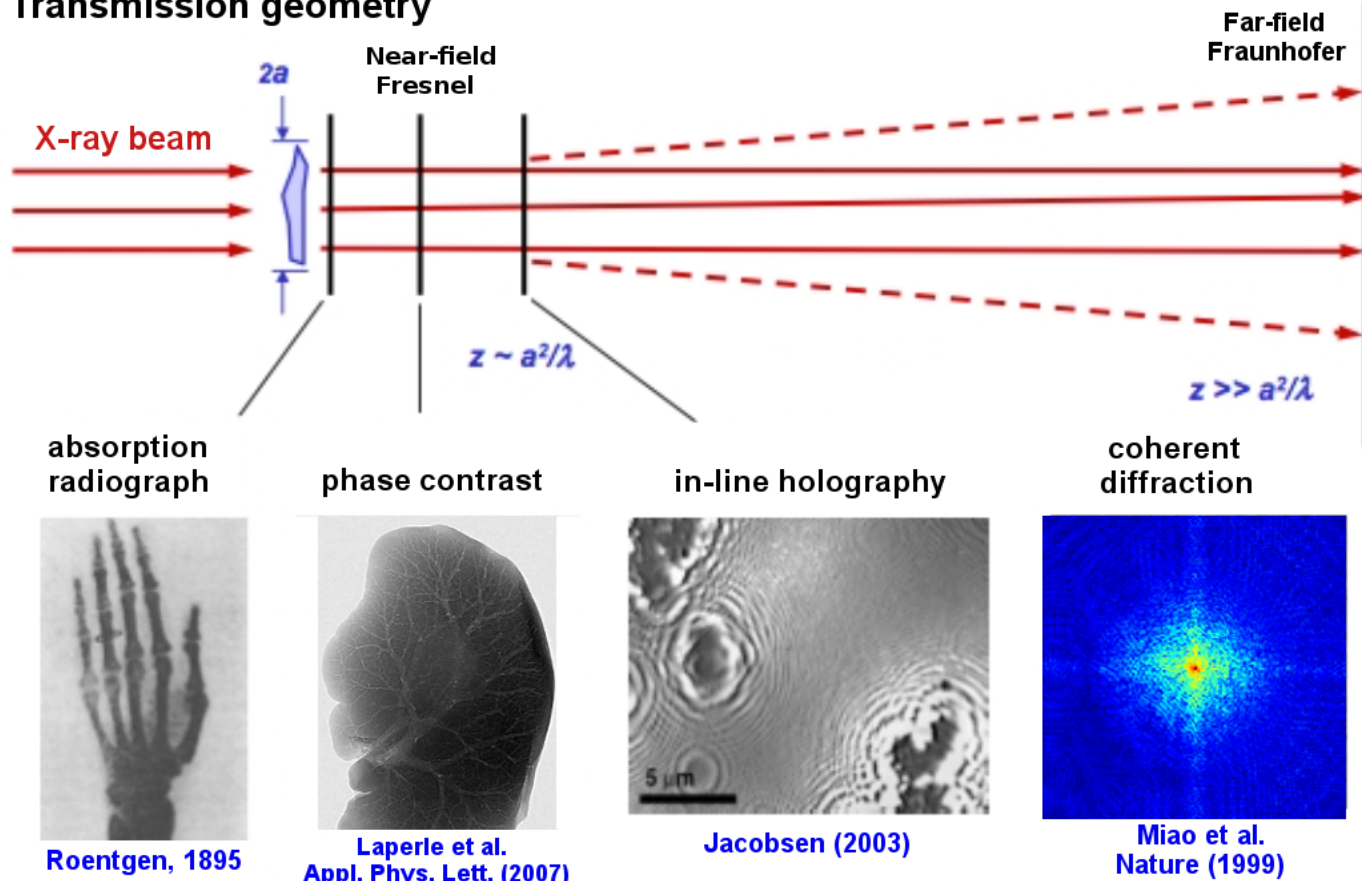


Phase shift

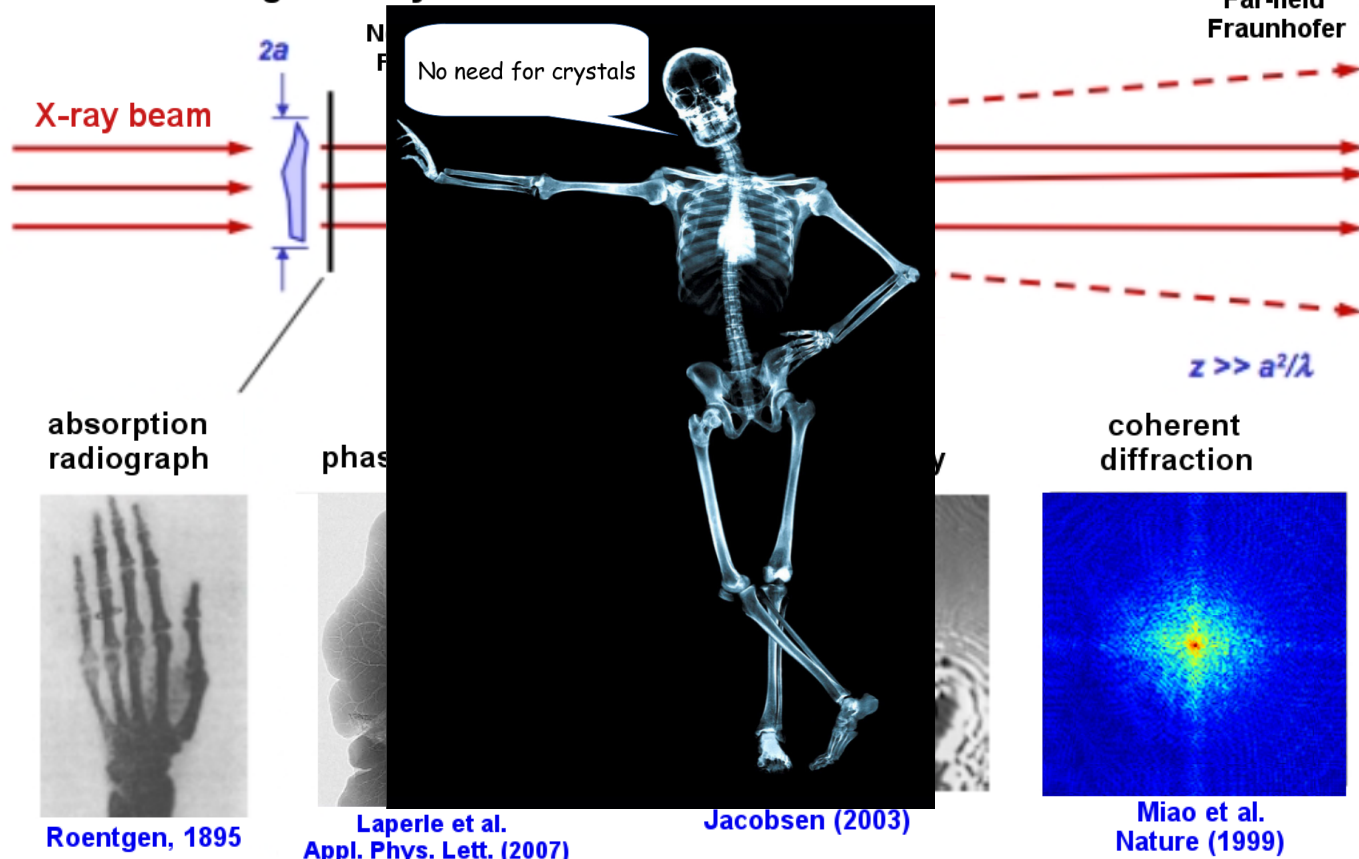


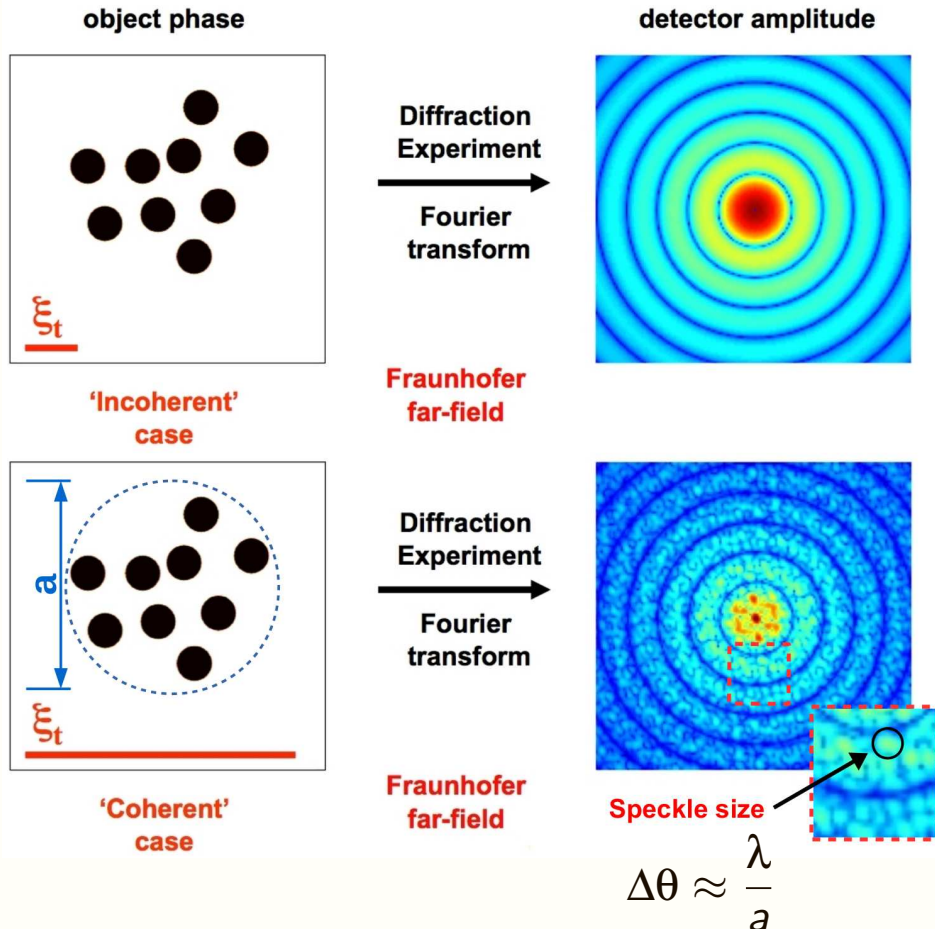


Transmission geometry

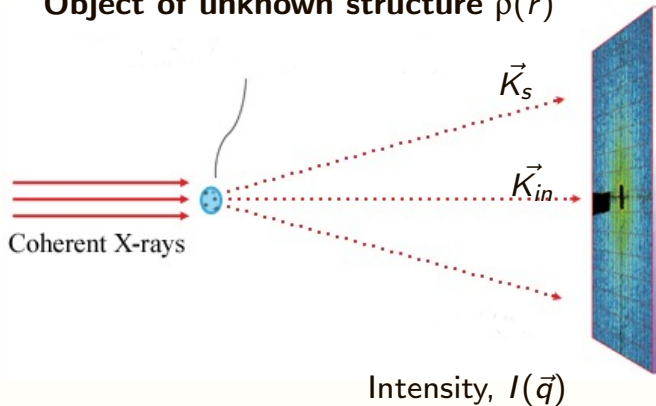


Transmission geometry





Object of unknown structure $\rho(\vec{r})$



Scattering vector

$$\vec{q} = \vec{k}_{\text{in}} - \vec{k}_s$$

Phase are lost

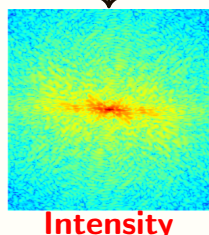
$$I(\vec{q}) = |E(\vec{q})|^2$$

$$E(\vec{q}) = |E(\vec{q})|e^{i\phi(\vec{q})}$$

Radiography



FT

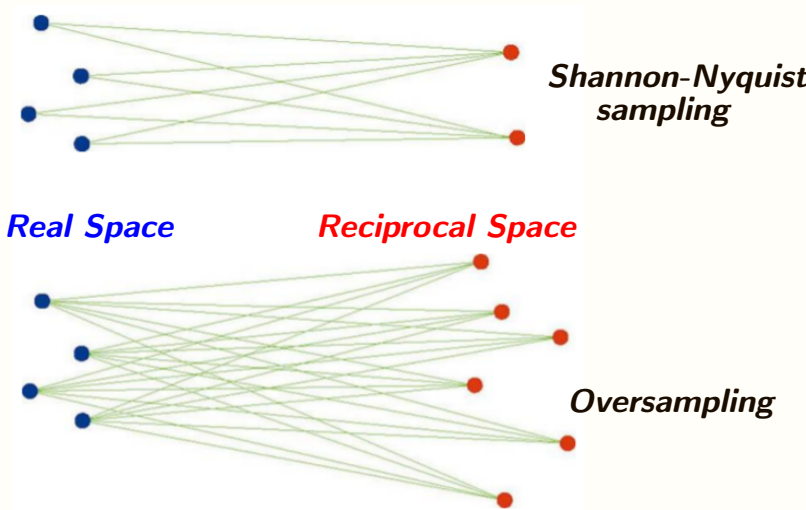


Images, yes... but, Fourier transformed ones

$$E(\vec{q}) = \underbrace{\int \rho(\vec{r}) e^{-2\pi i \vec{r} \cdot \vec{q}} d\vec{r}}_{\text{Fourier Transform}} = \mathcal{F}\{\rho(\vec{r})\}$$

Patterson Function: $\mathcal{F}\{|E(\vec{q})|^2\} = (\rho * \rho)(\vec{r}) = \int \rho(\vec{r}' + \vec{r}) \rho(\vec{r}') d\vec{r}'$

Oversampling of the intensities



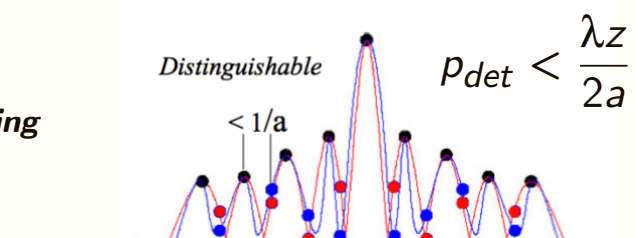
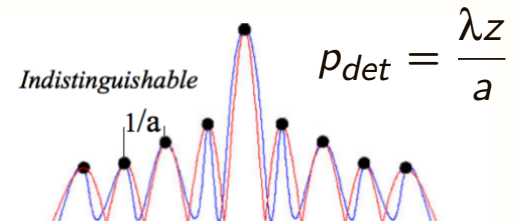
Sampling in the real space:

$$x \rightarrow \left[-\frac{L_x}{2} : \Delta x : \frac{L_x}{2} - \Delta x \right]$$

J. Goodman, Fourier Optics (book)

D. Sayre, Acta Cryst. 5, 843 (1952)

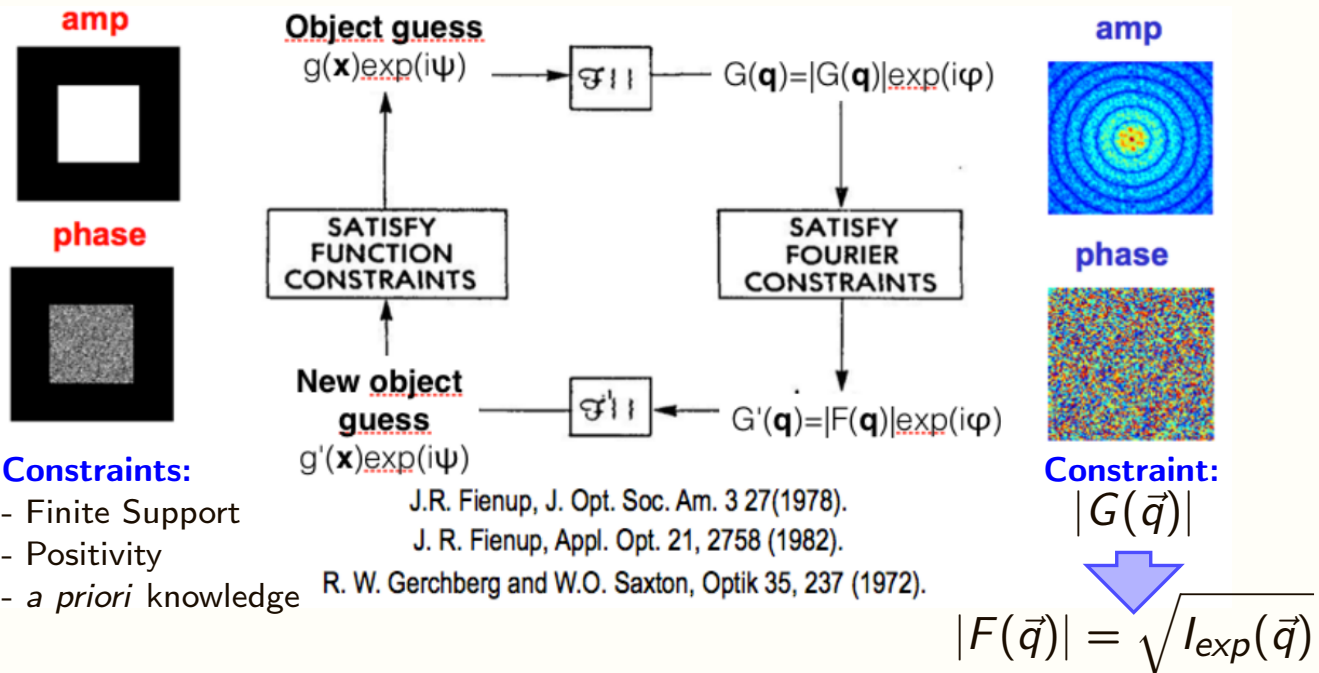
J. Miao, D. Sayre, H. Chapman, JOSA A 15, 1662 (1998)



Sampling in the Fourier Space:

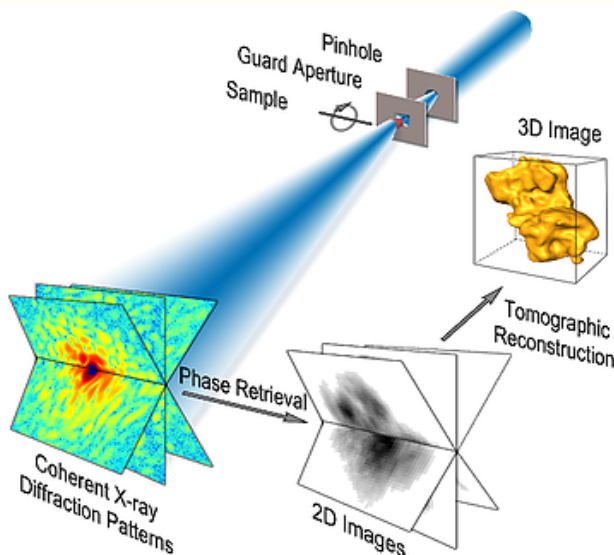
$$f_x \rightarrow \left[-\frac{1}{2\Delta x} : \frac{1}{L_x} : \frac{1}{2\Delta x} - \frac{1}{L_x} \right]$$

$$f_{Nyquist} = \frac{1}{2\Delta x}$$

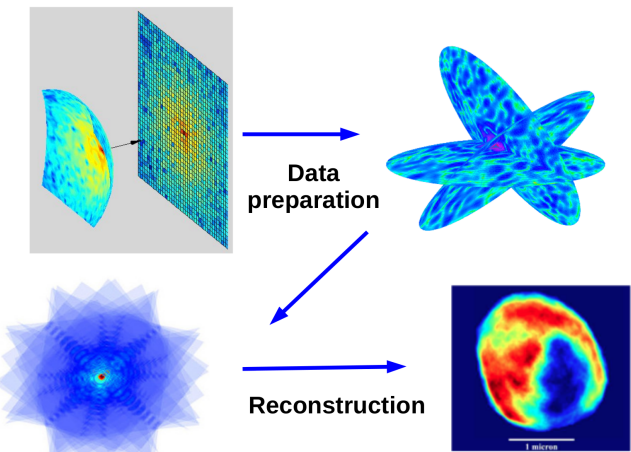


We cycle iteratively between Real and Reciprocal space through Fourier Transformations while imposing the constraints of each space until convergence is reached.

Tomo CDI



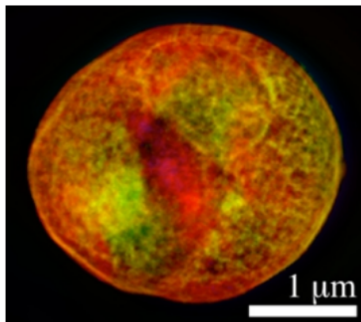
3D CDI



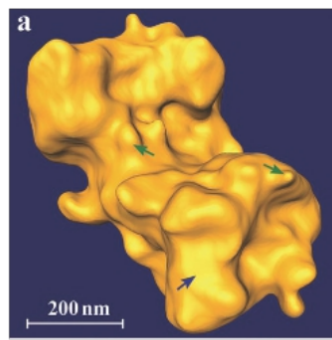
Some examples in the literature



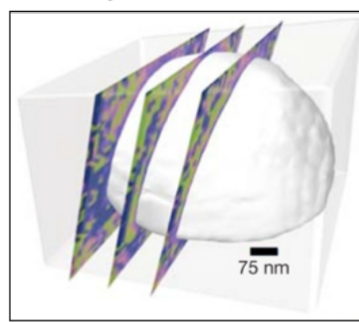
Miao et al. (1999)
Nature **400** 342.



Shapiro et al. (2005)
Proc. Natl. Acad. Sci. **102** 15343.



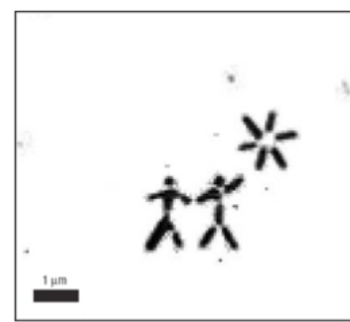
Miao et al. (2006)
Phys Rev Lett **97** 215503.



Pfeifer et al. (2006)
Nature **442** 63.



Chapman et al. (2006)
J. Opt. Soc. Am. A **23** 1179.



Chapman et al. (2006)
Nature Physics **2** 839.

Jupyter Notebook

CDI poses some challenges for detector technology

- very high dynamic range

- small pixel size and very large active detection area

- noise-free detectors

CDI poses some challenges for detector technology

- very high dynamic range
- small pixel size and very large active detection area
- noise-free detectors

Isolated particles

- specimens need to be isolated
- limited to small specimens
- tremendous oversampling of the intensities

CDI poses some challenges for detector technology

- very high dynamic range
- small pixel size and very large active detection area
- noise-free detectors

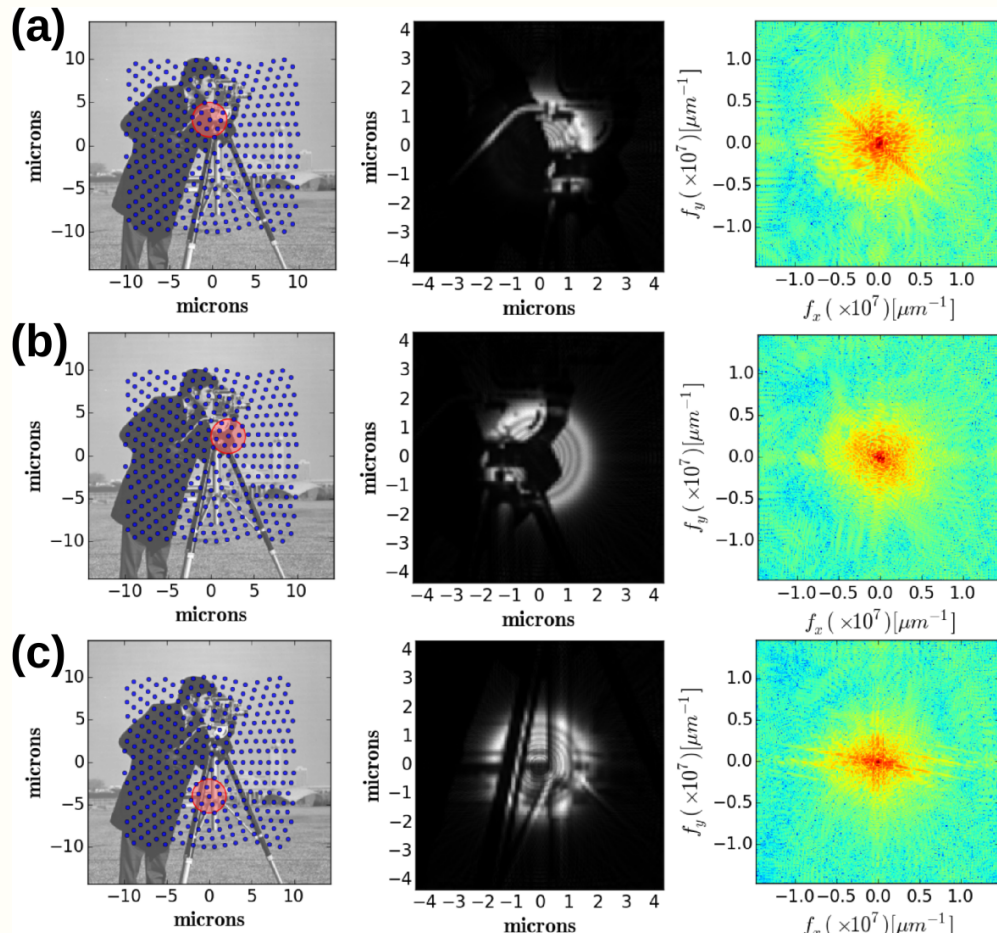
Isolated particles

- specimens need to be isolated
- limited to small specimens
- tremendous oversampling of the intensities

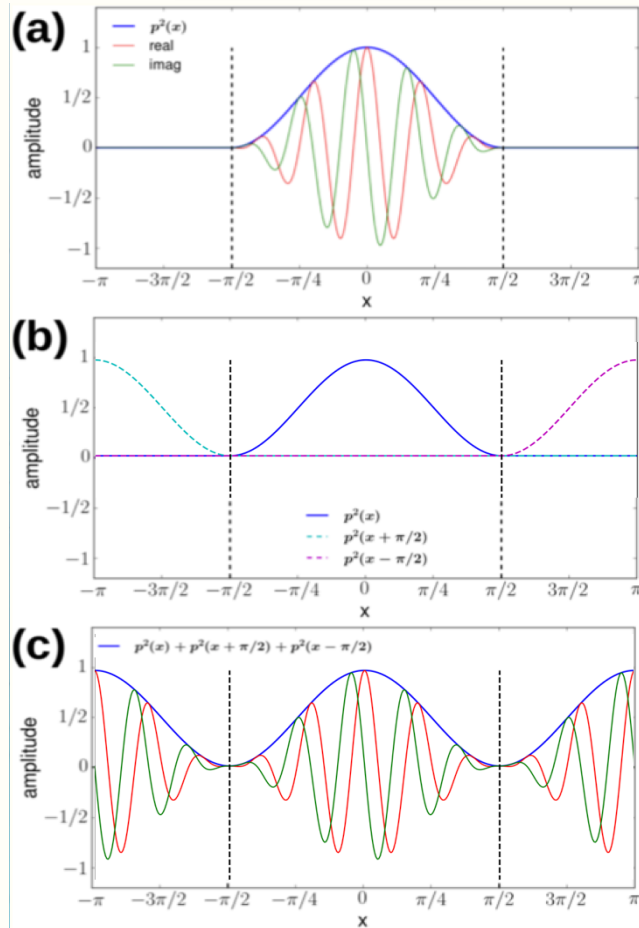
Algorithm stagnation problems

- slow convergence rate
- twin-images
- low-frequency information is hard to recover, but essential

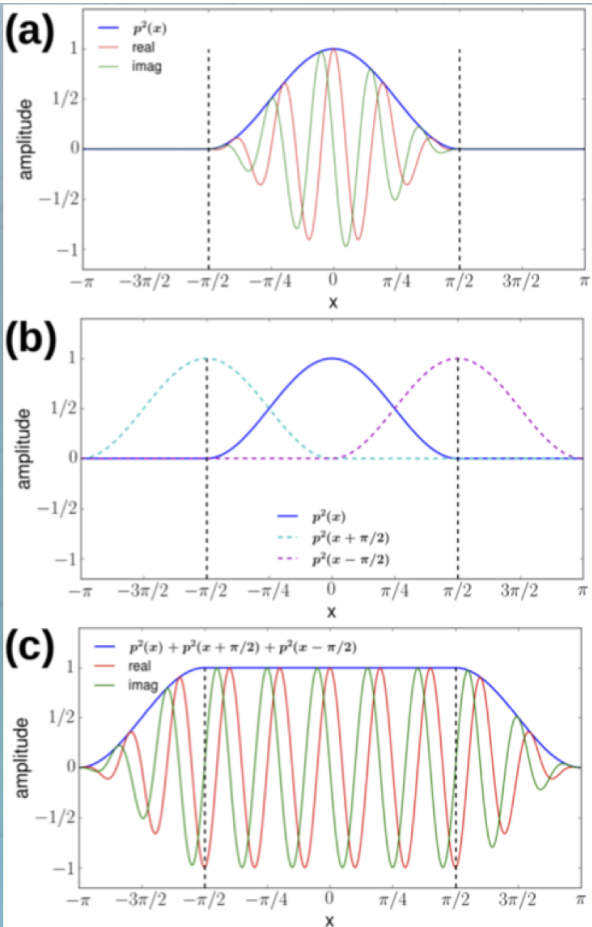
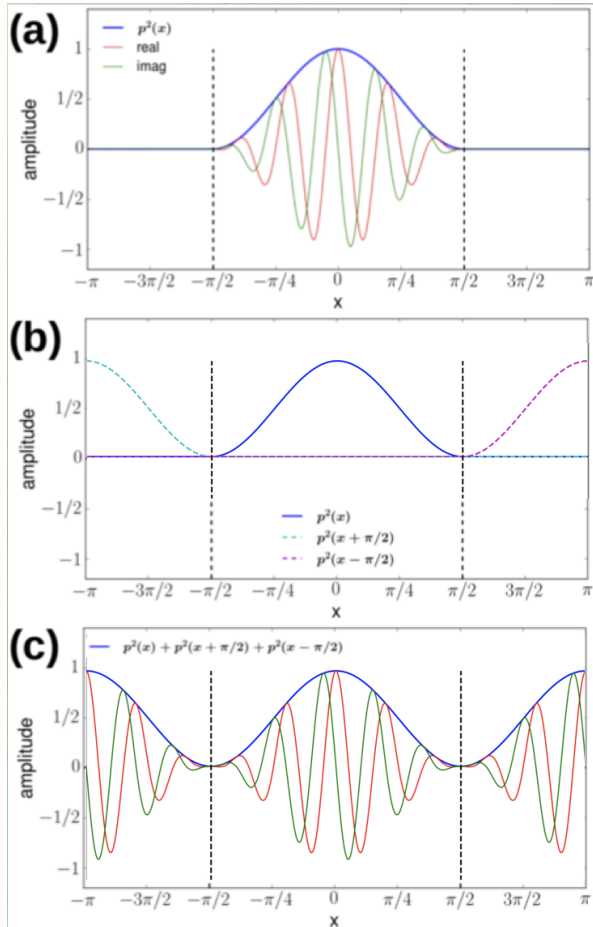
Developping a novel imaging technology

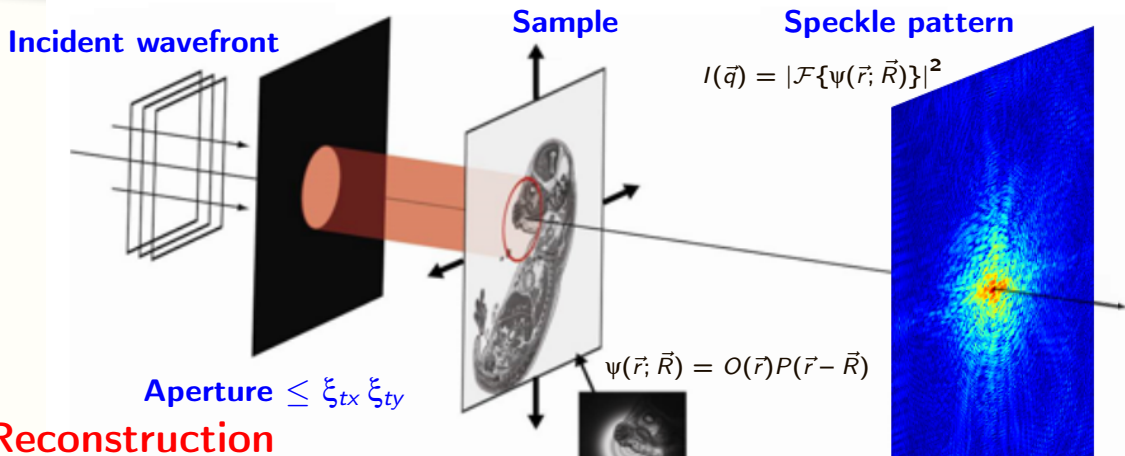


How to decide the step size for the scan?

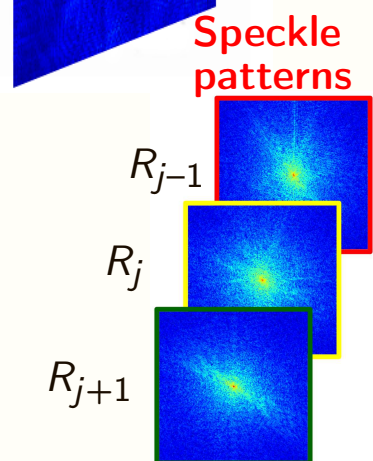
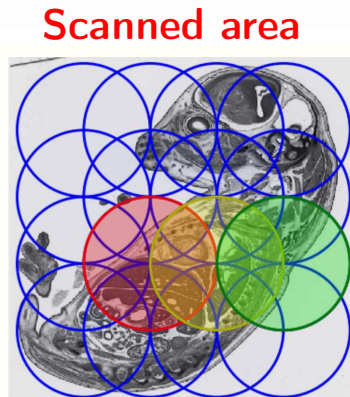
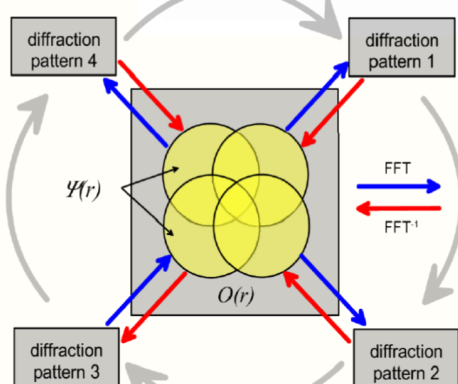


How to decide the step size for the scan?





Reconstruction algorithm



Pty·chog·ra·phy noun
from Greek: πτυξ = fold (crease)
and: γραφή = writing, drawing

German: Falte

1148

R. Hegerl und W. Hoppe: Dynamische Theorie der Kristallstrukturanalyse usw.

Berichte der
Bunsen-Gesellschaft

Dynamische Theorie der Kristallstrukturanalyse durch Elektronenbeugung im inhomogenen Primärstrahlwellenfeld

Von R. Hegerl und W. Hoppe

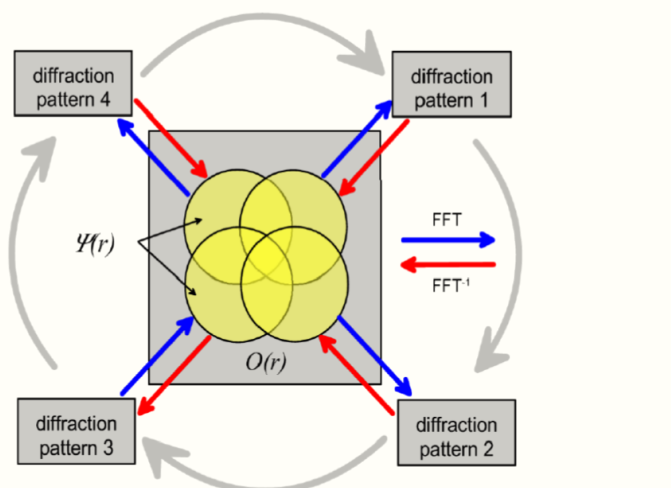
Some time ago a new principle was proposed for the registration of the complete information (amplitudes and phases) in a diffraction diagram, which does not—as does Holography—require the interference of the scattered waves with a single reference wave. The basis of the principle lies in the interference of neighbouring scattered waves which result when the object function $\varrho(x, y)$ is multiplied by a generalized primary wave function $p(x, y)$ in Fourier space (diffraction diagram) this is a convolution of the Fourier transforms of these functions. The above mentioned interferences necessary for the phase determination can be obtained by suitable choice of the shape of $p(x, y)$. To distinguish it from holography this procedure is designated “ptychography” ($\pi\tau\nu\xi$ = fold). The procedure is applicable to periodic and aperiodic structures. The relationships are simplest for plane lattices. In this paper the theory is extended to space lattices both with and without consideration of the dynamic theory. The resulting effects are demonstrated using a practical example.

Hoppe, Acta Cryst A 25 (1969) 508; Hegerl and Hoppe, Ber Physik Chemie 74 (1970) 1148

Find the object $O(r)$ and the complex-valued incident illumination $P(r)$ (the probe) consistent with the measured intensities:

$$I(\vec{q}; \vec{R}) = \left| \int_{-\infty}^{\infty} O(\vec{r}) P(\vec{r} - \vec{R}) e^{-i\vec{q} \cdot \vec{r}} d\vec{r} \right|^2$$

Iterative phase retrieval



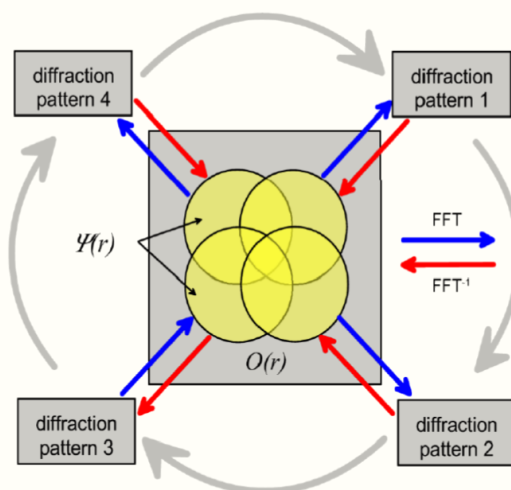
P. Thibault et al., Ultramicroscopy 4 (2009), 338.

H.M.L. Faulkner, J.M. Rodenburg, Phys. Rev. Lett. 93 (2004), 023903
J. C. da Silva and A. Menzel, Opt. Express 23 (2015) 33812.

Find the object $O(r)$ and the complex-valued incident illumination $P(r)$ (the probe) consistent with the measured intensities:

$$I(\vec{q}; \vec{R}) = \left| \int_{-\infty}^{\infty} O(\vec{r}) P(\vec{r} - \vec{R}) e^{-i\vec{q} \cdot \vec{r}} d\vec{r} \right|^2$$

Iterative phase retrieval



Fourier constraints

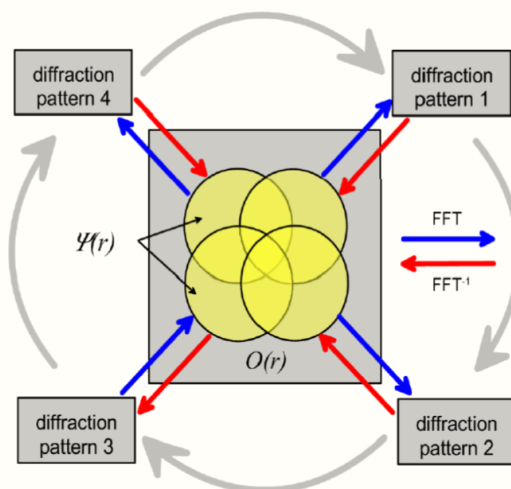
Each "view" satisfies its own Fourier constraint.

P. Thibault et al., Ultramicroscopy 4 (2009), 338.
H.M.L. Faulkner, J.M. Rodenburg, Phys. Rev. Lett. 93 (2004), 023903
J. C. da Silva and A. Menzel, Opt. Express 23 (2015) 33812.

Find the object $O(r)$ and the complex-valued incident illumination $P(r)$ (the probe) consistent with the measured intensities:

$$I(\vec{q}; \vec{R}) = \left| \int_{-\infty}^{\infty} O(\vec{r}) P(\vec{r} - \vec{R}) e^{-i\vec{q} \cdot \vec{r}} d\vec{r} \right|^2$$

Iterative phase retrieval



Fourier constraints

Each "view" satisfies its own Fourier constraint.

Overlap constraints

Overlapping regions agree and the incident wave field is unique.

P. Thibault et al., Ultramicroscopy 4 (2009), 338.

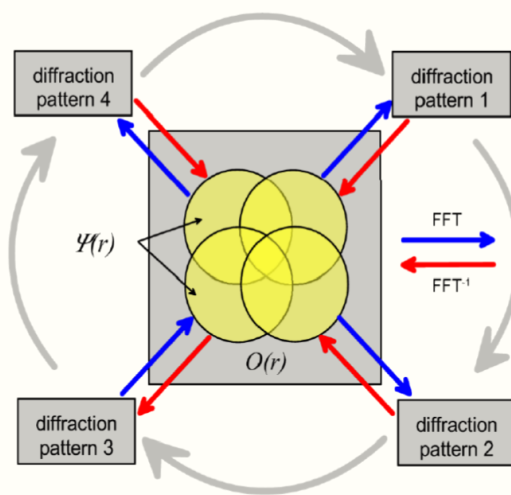
H.M.L. Faulkner, J.M. Rodenburg, Phys. Rev. Lett. 93 (2004), 023903

J. C. da Silva and A. Menzel, Opt. Express 23 (2015) 33812.

Find the object $O(r)$ and the complex-valued incident illumination $P(r)$ (the probe) consistent with the measured intensities:

$$I(\vec{q}; \vec{R}) = \left| \int_{-\infty}^{\infty} O(\vec{r}) P(\vec{r} - \vec{R}) e^{-i\vec{q} \cdot \vec{r}} d\vec{r} \right|^2$$

Iterative phase retrieval



Fourier constraints

Each "view" satisfies its own Fourier constraint.

Overlap constraints

Overlapping regions agree and the incident wave field is unique.

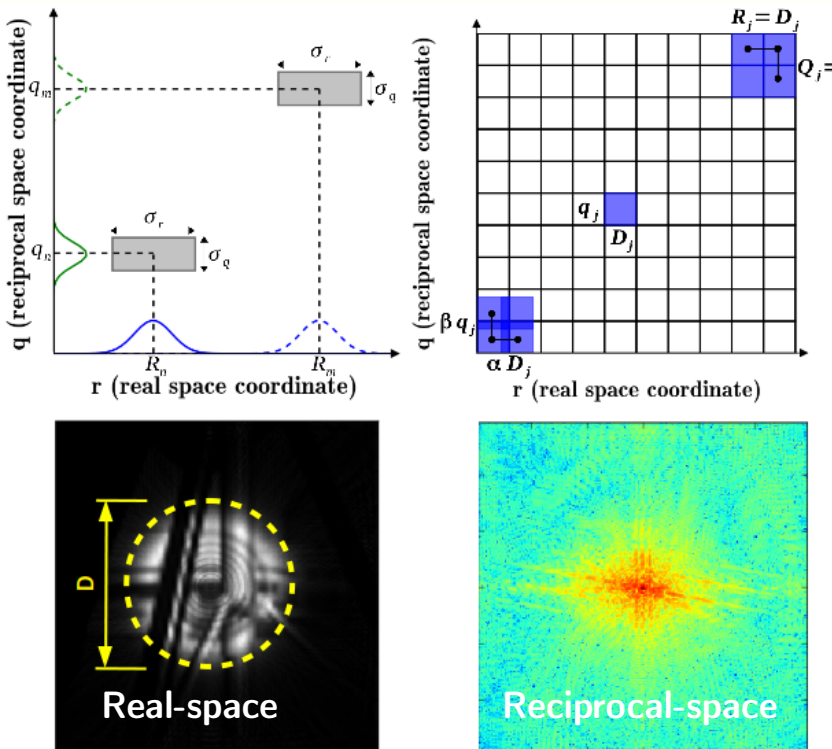
Redundancy

Allows to reconstruct the probe and the object.

P. Thibault et al., Ultramicroscopy 4 (2009), 338.

H.M.L. Faulkner, J.M. Rodenburg, Phys. Rev. Lett. 93 (2004), 023903

J. C. da Silva and A. Menzel, Opt. Express 23 (2015) 33812.



$$\psi(\vec{r}; \vec{R}) = O(\vec{r})P(\vec{r} - \vec{R})$$

$$I(\vec{q}) = |\mathcal{F}\{\psi(\vec{r}; \vec{R})\}|^2$$

J. C. da Silva, A. Menzel, Opt. Express 23 (2015) 33812.

Let us define:

$$R_j = \alpha D_j$$

$$Q_j = \beta q_j$$

$$\text{where: } \beta = \frac{1}{O}$$

Density of boxes:

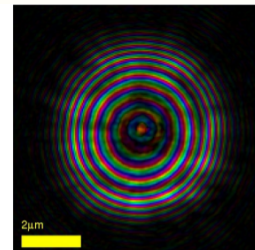
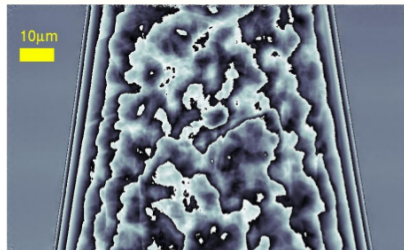
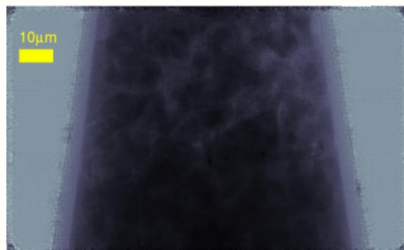
$$\frac{2\pi}{(\alpha D_j)(\beta q_j)} \geq 1$$

$$\boxed{\frac{1}{\alpha\beta} > 1}$$

Oversampling condition

Hydrated cement paste (Portland cement)

Amplitude Phase Probe

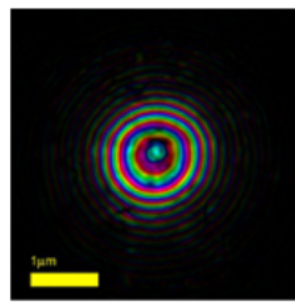
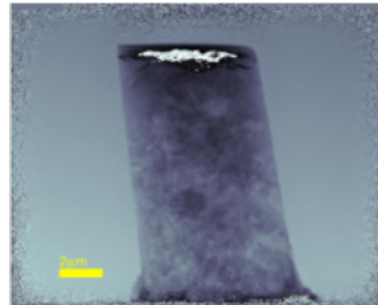
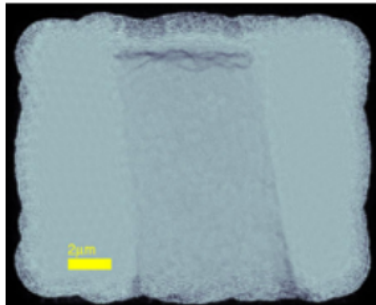


J. C. da Silva et al., *Langmuir* 31, (2015), 3779.

Color : phases
Brightness : amplitude

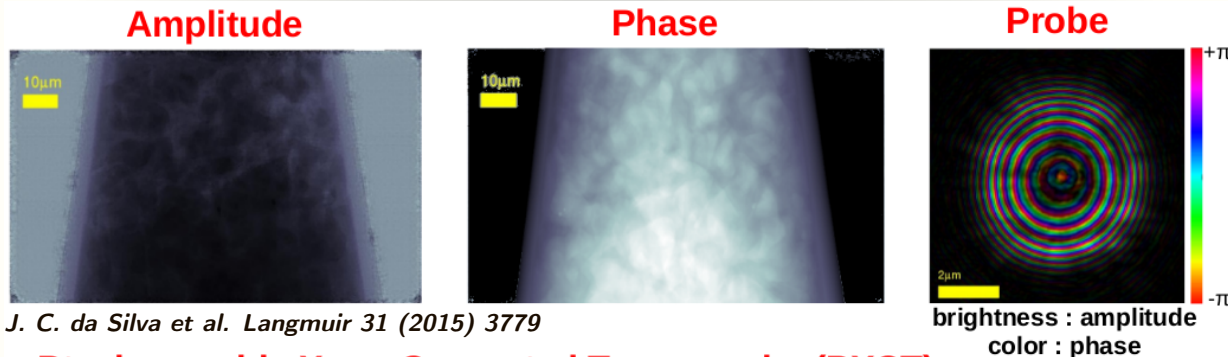
Fluid Catalyst Cracking (FCC) catalyst

Amplitude Phase Probe



J. C. da Silva et al., *ChemCatChem* 7, (2015), 413.

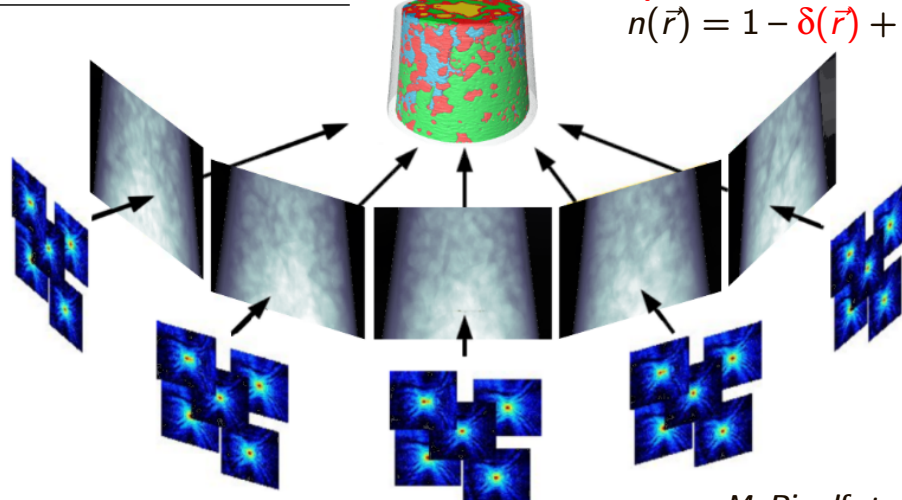
Jupyter Notebook



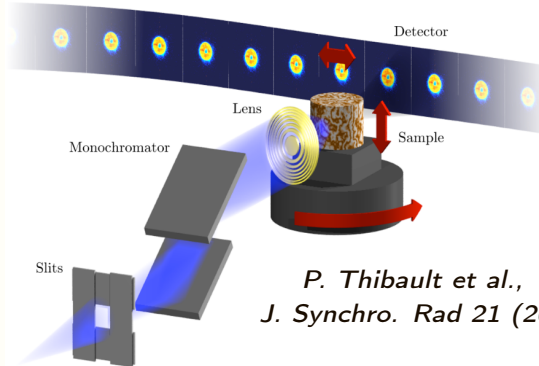
Ptychographic X-ray Computed Tomography (PXCT)

3D map of the refractive index

Complex-valued refractive index
 $n(\vec{r}) = 1 - \delta(\vec{r}) + i\beta(\vec{r})$

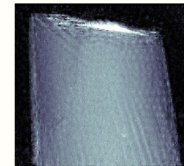


M. Dierolf et al. *Nature* 467 (2010) 436

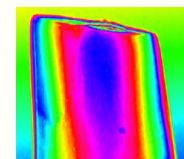


P. Thibault et al.,
J. Synchro. Rad 21 (2014) 1011.

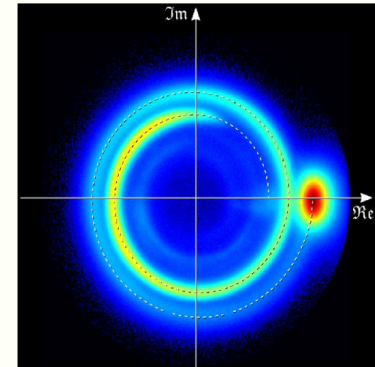
Amplitude



Phase



Complex domain



M. Dierolf et al., *Nature* 467 (2010) 436.

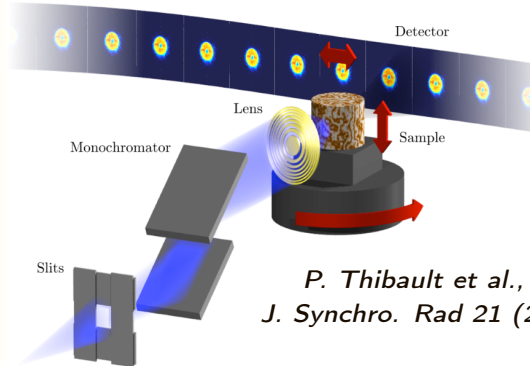
Refractive Index:

$$n(\vec{r}) = 1 - \delta(\vec{r}) + i\beta(\vec{r})$$

Complex Transmittance:

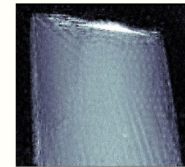
$$T(x, y) = \exp \left\{ \frac{2\pi i}{\lambda} \int [n(\vec{r}) - 1] dz \right\}$$

B. D. Cullity, *Elements of X-ray Diffraction*, Addison-Wesley Pub. Company, Inc. (1956)

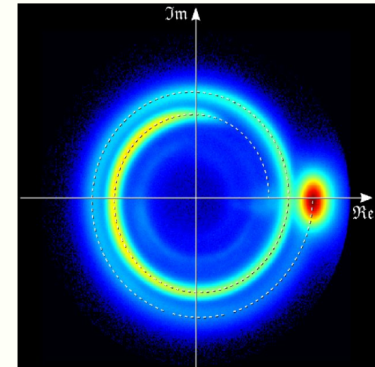


P. Thibault et al.,
J. Synchro. Rad 21 (2014) 1011.

Amplitude



Complex domain



M. Dierolf et al., *Nature* 467 (2010) 436.

Refractive Index:

$$n(\vec{r}) = 1 - \delta(\vec{r}) + i\beta(\vec{r})$$

Complex Transmittance:

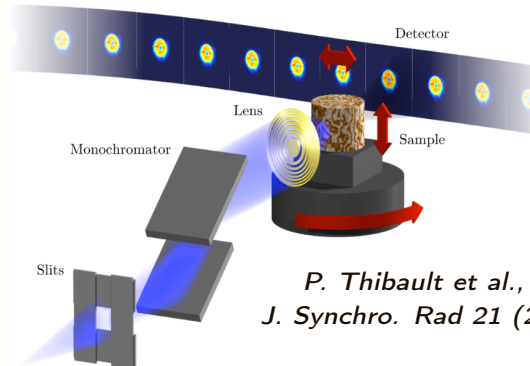
$$T(x, y) = \exp \left\{ \frac{2\pi i}{\lambda} \int [n(\vec{r}) - 1] dz \right\}$$

Attenuation

coefficient:

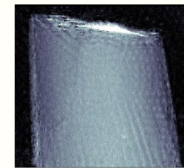
$$\mu(\vec{r}) = \left(\frac{4\pi}{\lambda} \right) \beta(\vec{r})$$

B. D. Cullity, *Elements of X-ray Diffraction*, Addison-Wesley Pub. Company, Inc. (1956)

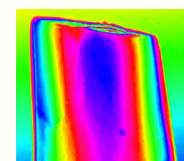


P. Thibault et al.,
J. Synchro. Rad 21 (2014) 1011.

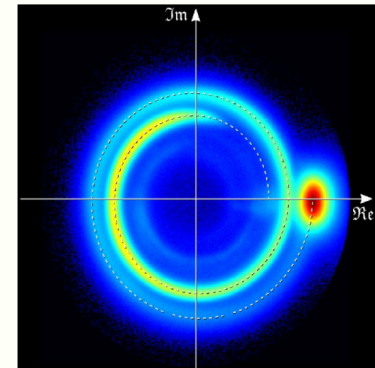
Amplitude



Phase



Complex domain



M. Dierolf et al., *Nature* 467 (2010) 436.

Refractive Index:

$$n(\vec{r}) = 1 - \delta(\vec{r}) + i\beta(\vec{r})$$

Complex Transmittance:

$$T(x, y) = \exp \left\{ \frac{2\pi i}{\lambda} \int [n(\vec{r}) - 1] dz \right\}$$

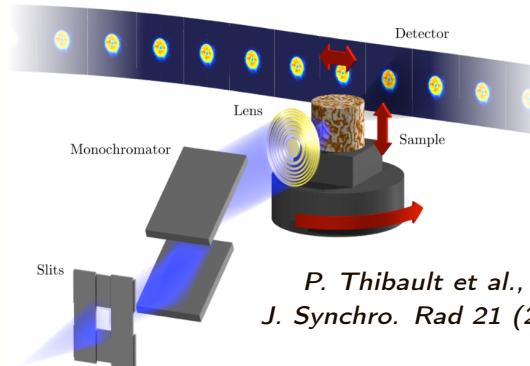
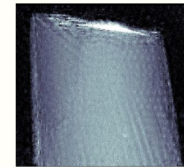
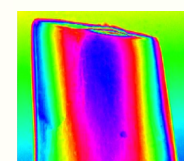
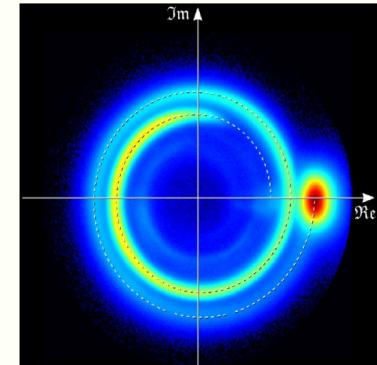
Attenuation coefficient:

$$\mu(\vec{r}) = \left(\frac{4\pi}{\lambda} \right) \beta(\vec{r})$$

Electron Density:

$$n_e(\vec{r}) = \frac{2\pi\delta(\vec{r})}{\lambda^2 r_0}$$

B. D. Cullity, *Elements of X-ray Diffraction*, Addison-Wesley Pub. Company, Inc. (1956)

**Amplitude****Phase****Complex domain***M. Dierolf et al., Nature 467 (2010) 436.***Refractive Index:**

$$n(\vec{r}) = 1 - \delta(\vec{r}) + i\beta(\vec{r})$$

Complex Transmittance:

$$T(x, y) = \exp \left\{ \frac{2\pi i}{\lambda} \int [n(\vec{r}) - 1] dz \right\}$$

Attenuation coefficient:

$$\mu(\vec{r}) = \left(\frac{4\pi}{\lambda} \right) \beta(\vec{r})$$

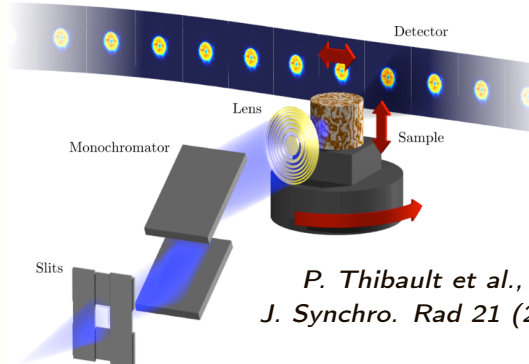
Electron Density:

$$n_e(\vec{r}) = \frac{2\pi\delta(\vec{r})}{\lambda^2 r_0}$$

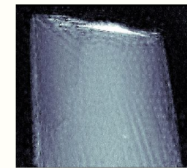
Mass density:

$$\rho(\vec{r}) = \frac{n_e(\vec{r})}{N_A} \left(\frac{\sum_i \alpha_i A_i}{\sum_i \alpha_i Z_i} \right)$$

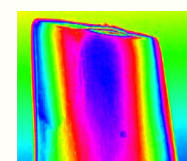
B. D. Cullity, Elements of X-ray Diffraction, Addison-Wesley Pub. Company, Inc. (1956)



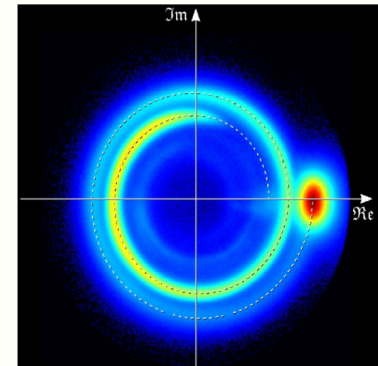
Amplitude



Phase



Complex domain



M. Dierolf et al., Nature 467 (2010) 436.

Refractive Index:

$$n(\vec{r}) = 1 - \delta(\vec{r}) + i\beta(\vec{r})$$

Complex Transmittance:

$$T(x, y) = \exp \left\{ \frac{2\pi i}{\lambda} \int [n(\vec{r}) - 1] dz \right\}$$

Attenuation coefficient:

$$\mu(\vec{r}) = \left(\frac{4\pi}{\lambda} \right) \beta(\vec{r})$$

Electron Density:

$$n_e(\vec{r}) = \frac{2\pi\delta(\vec{r})}{\lambda^2 r_0}$$

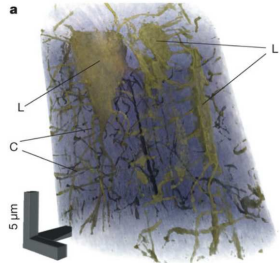
Mass density:

$$\rho(\vec{r}) = \frac{n_e(\vec{r})}{N_A} \left(\frac{\sum_i \alpha_i A_i}{\sum_i \alpha_i Z_i} \right)$$

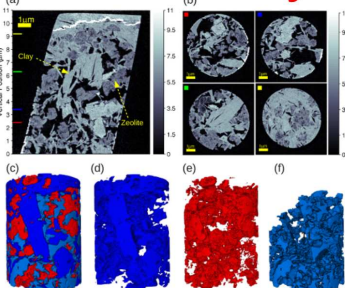
Mass attenuation coefficient:

$$\frac{\mu}{\rho} = k\lambda^3 Z^3$$

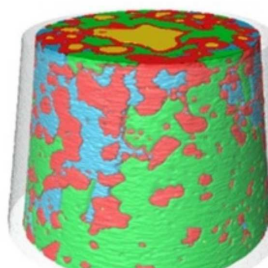
B. D. Cullity, Elements of X-ray Diffraction, Addison-Wesley Pub. Company, Inc. (1956)

Bone

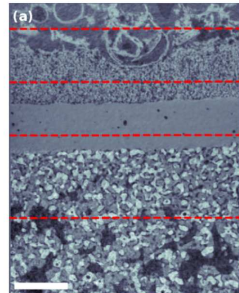
M. Dierolf et al.,
Nature 467 (2010) 436.

Technical catalyst

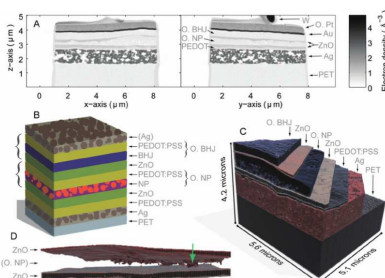
J. C. da Silva et al.,
ChemCatChem 7 (2015) 413.

Cement

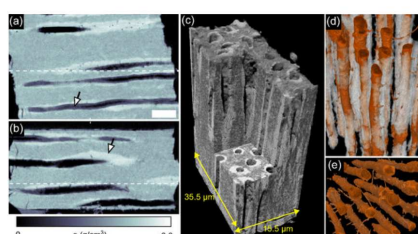
J. C. da Silva et al.,
Langmuir 31 (2015) 3779.

SOFC

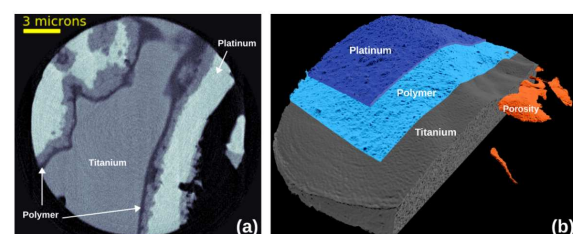
M. Stockmar et al.,
Opt. Express 23 (2015) 12720.

Tandem solar cell

E. B. L. Pedersen et al.,
Nanoscale 7 (2015) 13765.

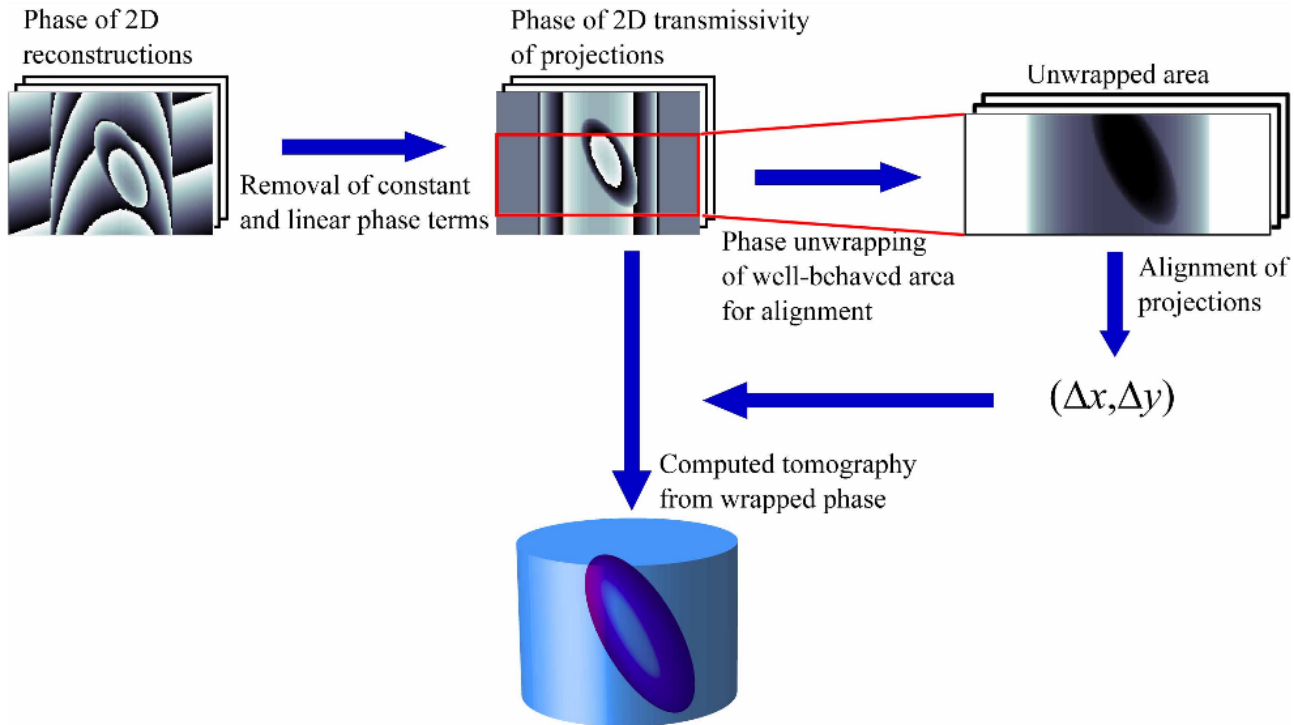
Human dentine

I. Zanette et al.,
Sci. Rep. 5 (2015) 9210.

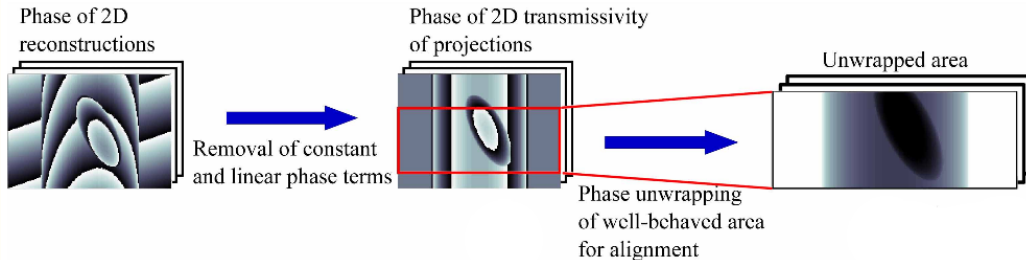
Polymer-metal welding

J. Haubrich et al.,
Appl. Surf. Sci. 433 (2018) 546.

PXCT - Pre-processing steps



M. Guizar-Sicairos et al., Opt. Express 19 (2011) 21345.



Complex-valued transmittance of the sample

$$T(x, y, \theta) = \exp \left\{ \frac{2\pi i}{\lambda} \int [n(\vec{r}') - 1] dz \right\}$$

$$\vec{r}' = (x \cos \theta - z \sin \theta, y, z \cos \theta + x \sin \theta)$$

Sample (object)

$$O(x, y, \theta) = T(x, y, \theta) e^{[i(a_\theta + b_\theta x + c_\theta y)]}$$

where the constants are:

a_θ = indeterminacy of absolute phase

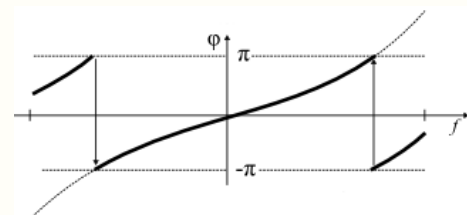
b_θ and c_θ = indeterminacy of the center of the diffraction pattern

M. Guizar-Sicairos et al., Opt. Express 19 (2011) 21345.

Obtaining the phases:

$$\phi(x, y, \theta) = \arg[T(x, y, \theta)] = -\frac{2\pi}{\lambda} \int \delta(\vec{r}') dz$$

1D wrapping



Wrapped phase image



After wrapping a region



2D phase wrapping / unwrapping

Algorithms:

→ Herraez's algorithm

(*J. Appl. Opt.* 41 (2002) 7437)

→ Goldstein's algorithm

(*M. Goldstein et al., Radio Sci.* 23 (1988) 713)

→ Flynn's algorithm

(*T. J. Flynn, J. Opt. Soc. Am. A* 14 (1997) 2692)

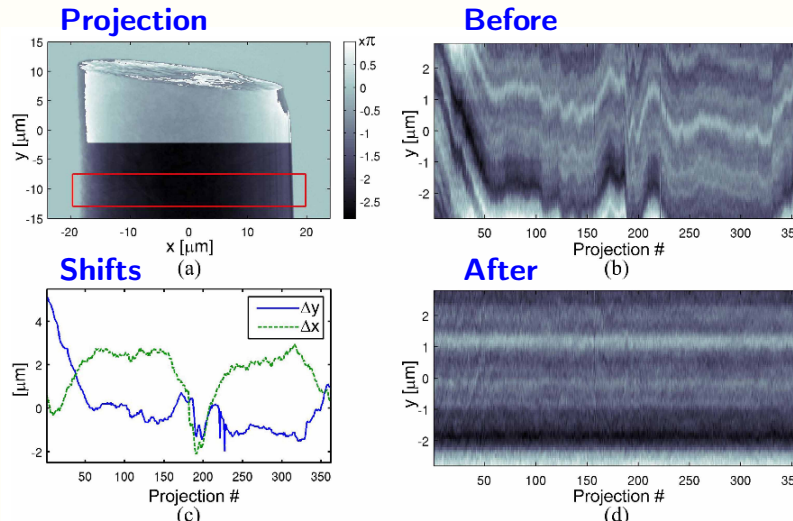
D. C. Ghiglia and M. D. Pritt, *Two-Dimensional Phase Unwrapping: Theory, Algorithms and Software*. New York: Wiley-Interscience, 1998.

Vertical "mass" distribution:

$$M_\theta(y) = \int \phi(x, y, \theta) dx = -\frac{2\pi}{\lambda} \iint \delta(x \cos \theta - z \sin \theta, y, z \cos \theta + x \sin \theta) dx dz$$

which is independent of the angle due to the Plancherel's theorem for Radon transform: $\int R(f)(\theta, p) dp = \iint f(x, z) dx dz$

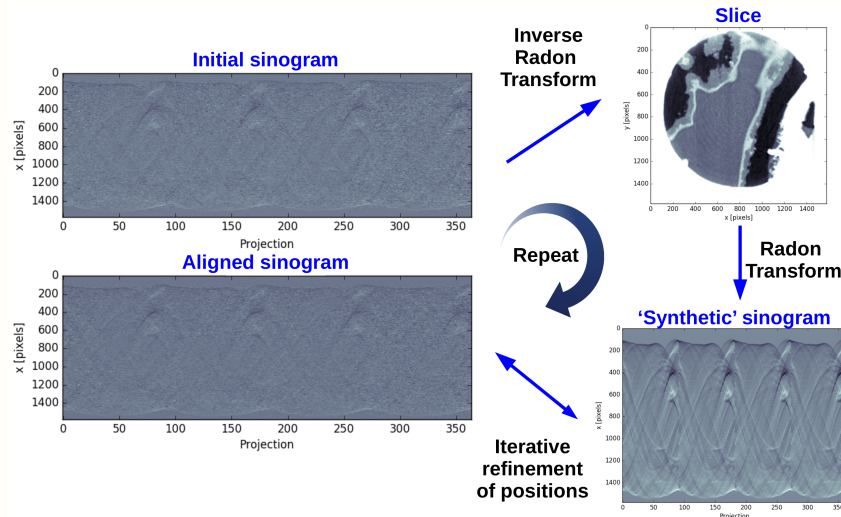
T. S. Durrani, D. Bisset, "The Radon transform and its properties", Geophysics 49 (1984) 1180.



M. Guizar-Sicairos et al., Opt. Express 19 (2011) 21345.

Tomographic consistency:

"The inverse Radon transform by FBP followed by a Radon transform only retrieves the original sinograms if they are consistent with a 3D representation, which is not the case for misaligned projections."



M. Guizar-Sicairos et al., Optica 2 2015) 259.

S. Mayo et al, J. Microsc. 228 (2007) 257.

J. Dengler, Ultramicroscopy 30 (1989) 337.

"Traditional" Filtered back projection (FBP):

(R. N. Bracewell, A. C. Riddle, *The Astrophysical J.* 150 (1967) 427)

$$-\frac{2\pi\Delta}{\lambda}\delta(\vec{r}) = \int_0^\pi \mathcal{F}_u^{-1}\{|u|\mathcal{F}_{x'}\{\phi(x', y, \theta)\}\}d\theta$$

where Δ is the length of the side of the voxel.

"Traditional" Filtered back projection (FBP):

(R. N. Bracewell, A. C. Riddle, *The Astrophysical J.* 150 (1967) 427)

$$-\frac{2\pi\Delta}{\lambda}\delta(\vec{r}) = \int_0^\pi \mathcal{F}_u^{-1}\{|u|\mathcal{F}_{x'}\{\phi(x', y, \theta)\}\}d\theta$$

where Δ is the length of the side of the voxel.

Using the derivative property of the Fourier transform: $\mathcal{F}_x\{\partial\phi/\partial x\} = i2\pi u \mathcal{F}_x\{\phi\}$

"Traditional" Filtered back projection (FBP):
(R. N. Bracewell, A. C. Riddle, *The Astrophysical J.* 150 (1967) 427)

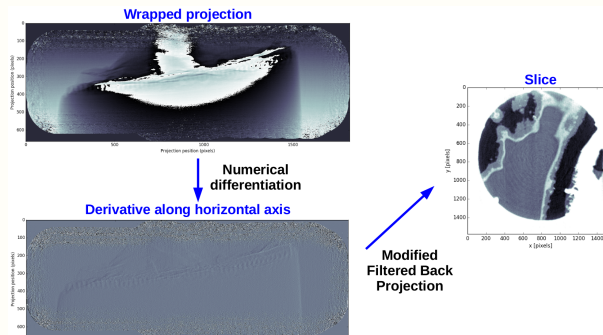
$$-\frac{2\pi\Delta}{\lambda}\delta(\vec{r}) = \int_0^\pi \mathcal{F}_u^{-1}\{|u|\mathcal{F}_{x'}\{\phi(x', y, \theta)\}\}d\theta$$

where Δ is the length of the side of the voxel.

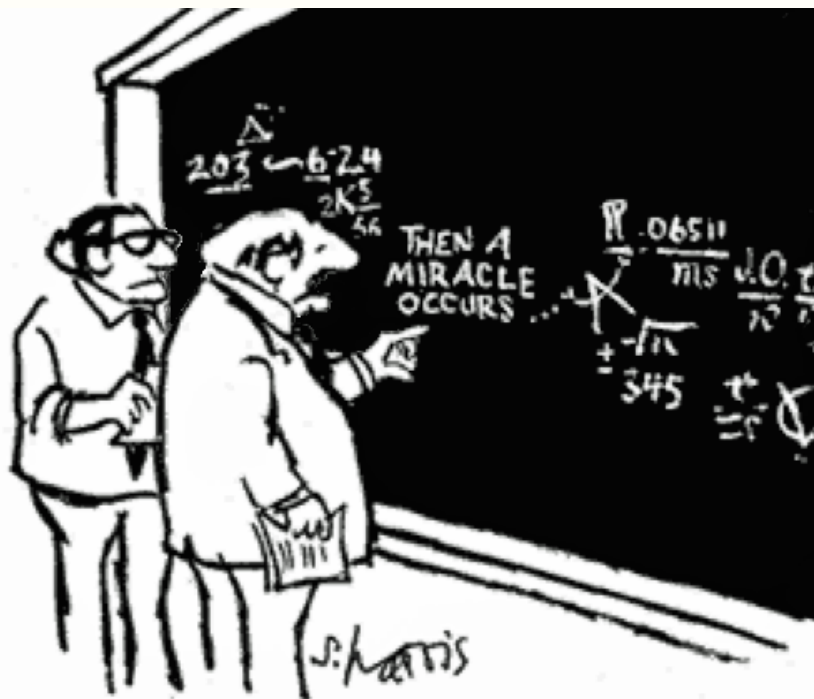
Using the derivative property of the Fourier transform: $\mathcal{F}_x\{\partial\phi/\partial x\} = i2\pi u \mathcal{F}_x\{\phi\}$

Modified Filtered back projection (FBP)

$$-\frac{2\pi\Delta}{\lambda}\delta(\vec{r}) = \int_0^\pi \mathcal{F}_u^{-1}\left\{\frac{1}{i2\pi \operatorname{sgn}(u)}\mathcal{F}_x\left\{\frac{\partial\phi(x, y, \theta)}{\partial x}\right\}\right\}d\theta$$

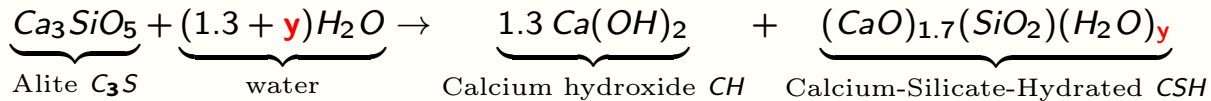
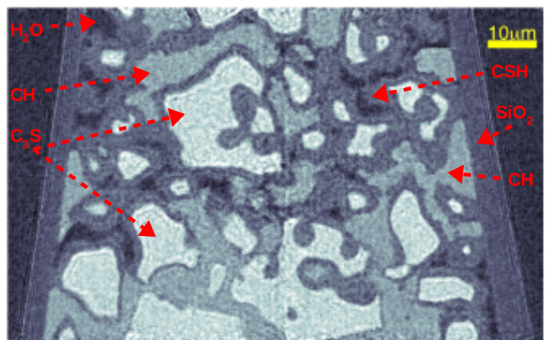
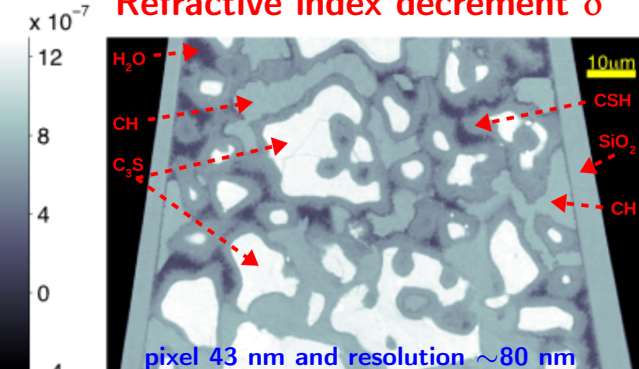


M. Guizar-Sicairos et al., *Opt. Express* 19 (2011) 21345.



"I THINK YOU SHOULD BE MORE EXPLICIT HERE IN STEP TWO."

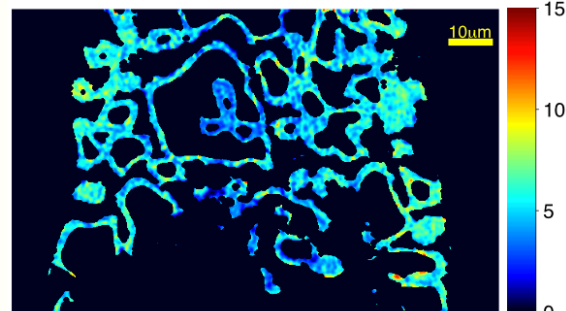
Jupyter Notebook

Absorption index β Refractive index decrement δ 

$$\left(\frac{\mu}{\rho}\right)_{CSH} = \omega_{CaO} \left(\frac{\mu}{\rho}\right)_{CaO} + \omega_{SiO_2} \left(\frac{\mu}{\rho}\right)_{SiO_2} + \omega_{H_2O} \left(\frac{\mu}{\rho}\right)_{H_2O}$$

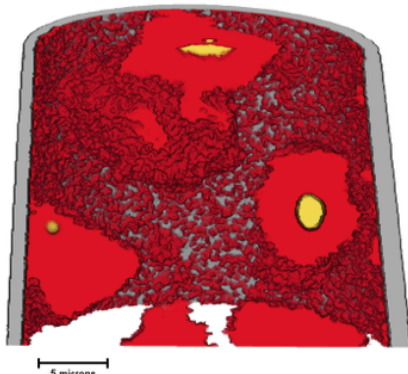
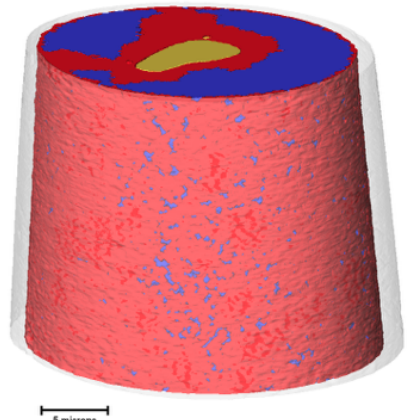
Materials	ρ ($g.cm^{-3}$)	$\rho_{ex.}$ ($g.cm^{-3}$)
Water	0.99 ± 0.01	1.00
CH	2.18 ± 0.01	2.211
C_3S	3.10 ± 0.01	3.064
Capillary	2.19 ± 0.01	2.203
$CSH_{(y=5.2 \pm 0.4)}$	1.83 ± 0.01	$1.83 (y = 5)$

Water content of CSH:



J. C. da Silva et al., Langmuir 31 (2015) 3779.

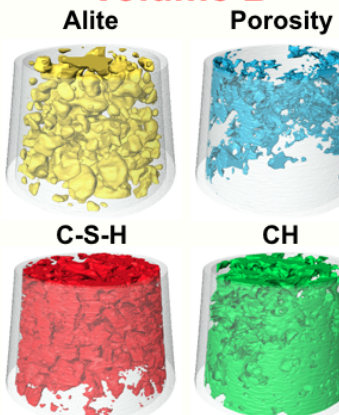
How the phases are seated to each other

Volume A

C-S-H

Porosity

Alite

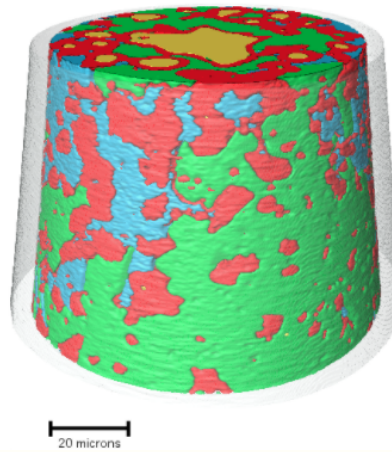
Volume B

Alite

Porosity

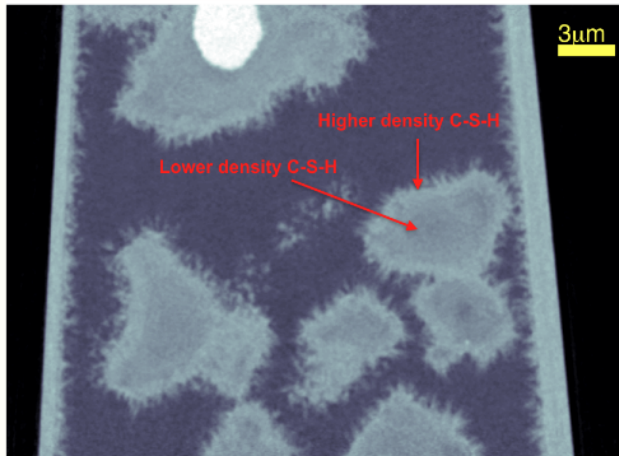
C-S-H

CH

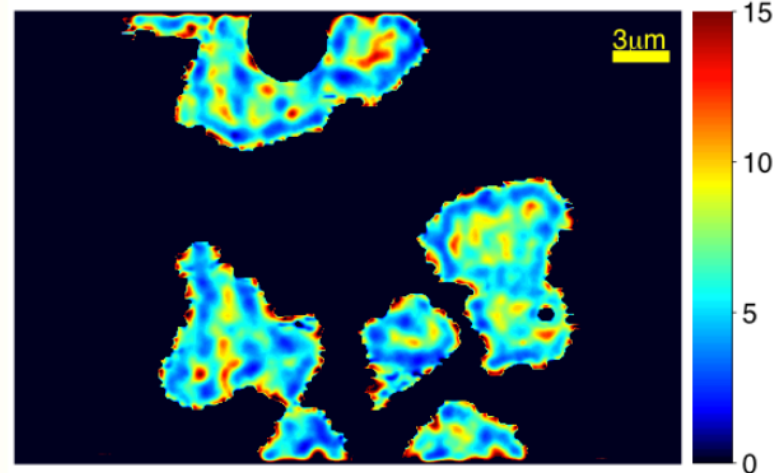


J. C. da Silva et al., Langmuir 31, (2015), 3779.

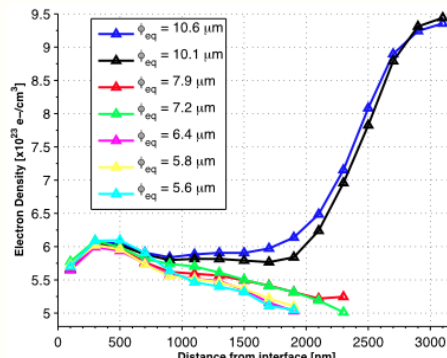
High and low density CSH



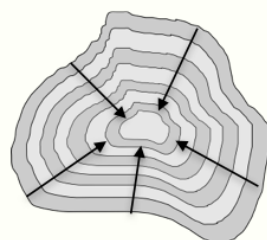
Water content of CSH



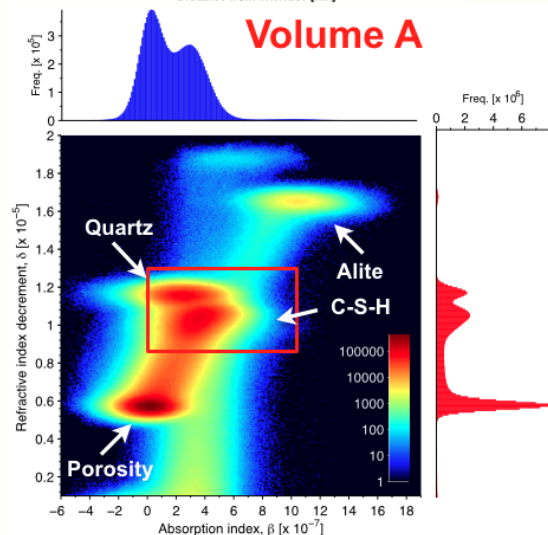
J. C. da Silva et al., Langmuir 31, (2015), 3779.



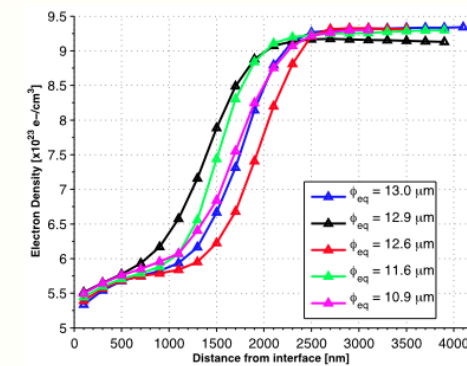
Distances in 3D



Shell of 200 nm



Volume A



Volume B

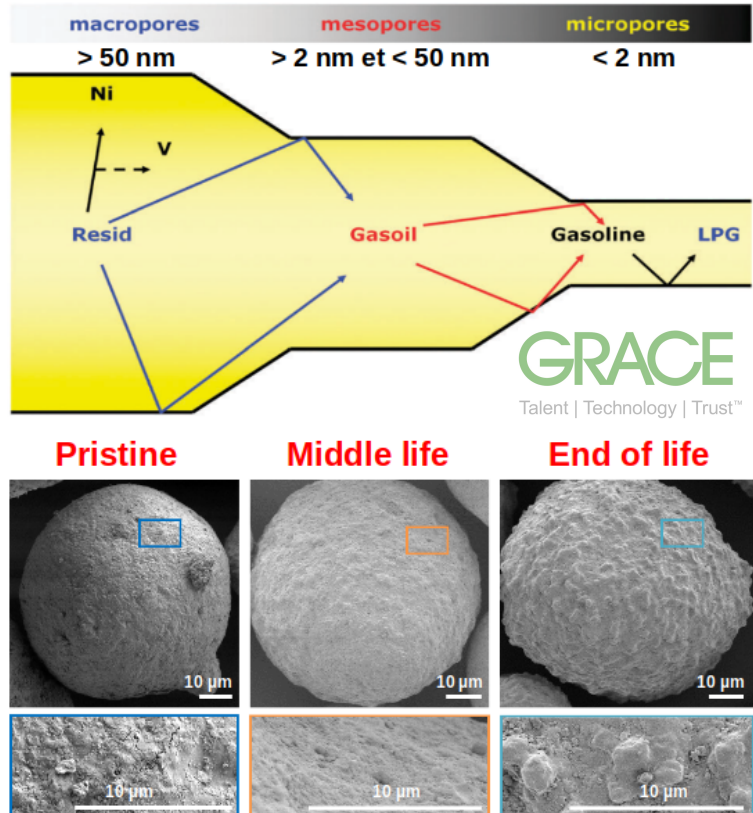
The greenhouse effect



Acid rain

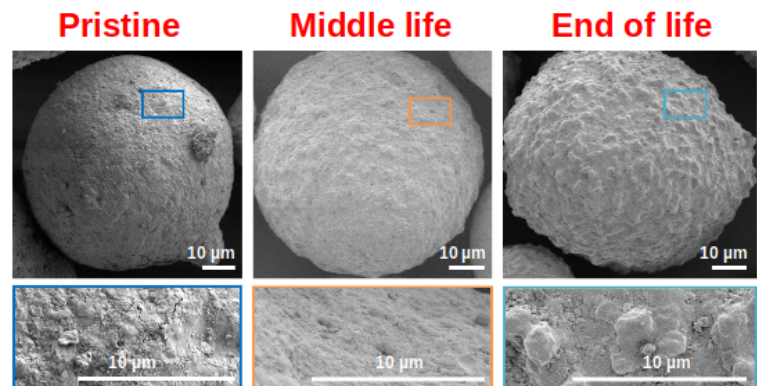


Fluid Catalytic Cracking catalyst (FCC)



J. Ihli,..., J.C. da Silva et al., *Nature Communications* 8, 809 (2017).
J. C. da Silva et al., *ChemCatChem* 7, 413 (2015).

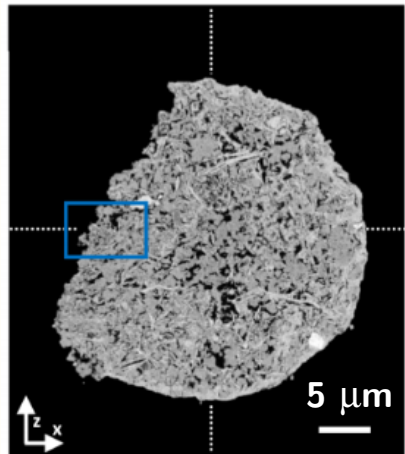
Fluid Catalytic Cracking catalyst (FCC)



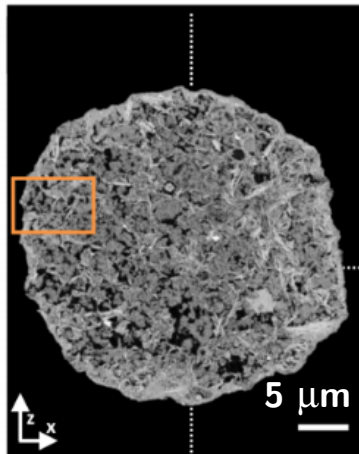
J. Ihli,..., J.C. da Silva et al., *Nature Communications* 8, 809 (2017).
J. C. da Silva et al., *ChemCatChem* 7, 413 (2015).

Characterization of FCC catalyst bodies via PXCT

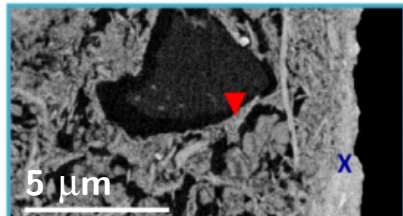
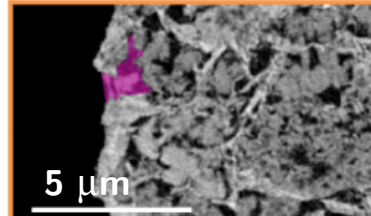
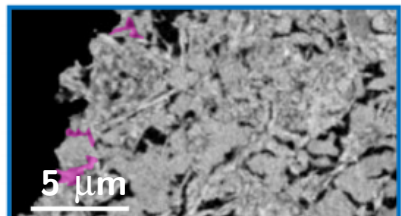
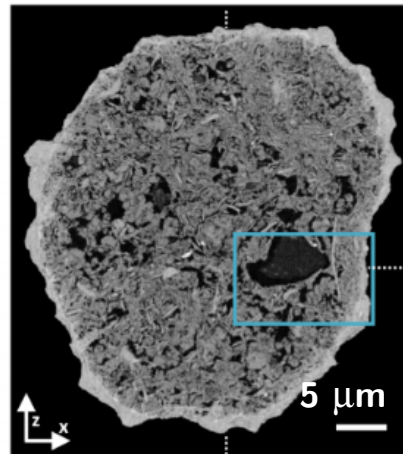
pristine



middle life



end of life

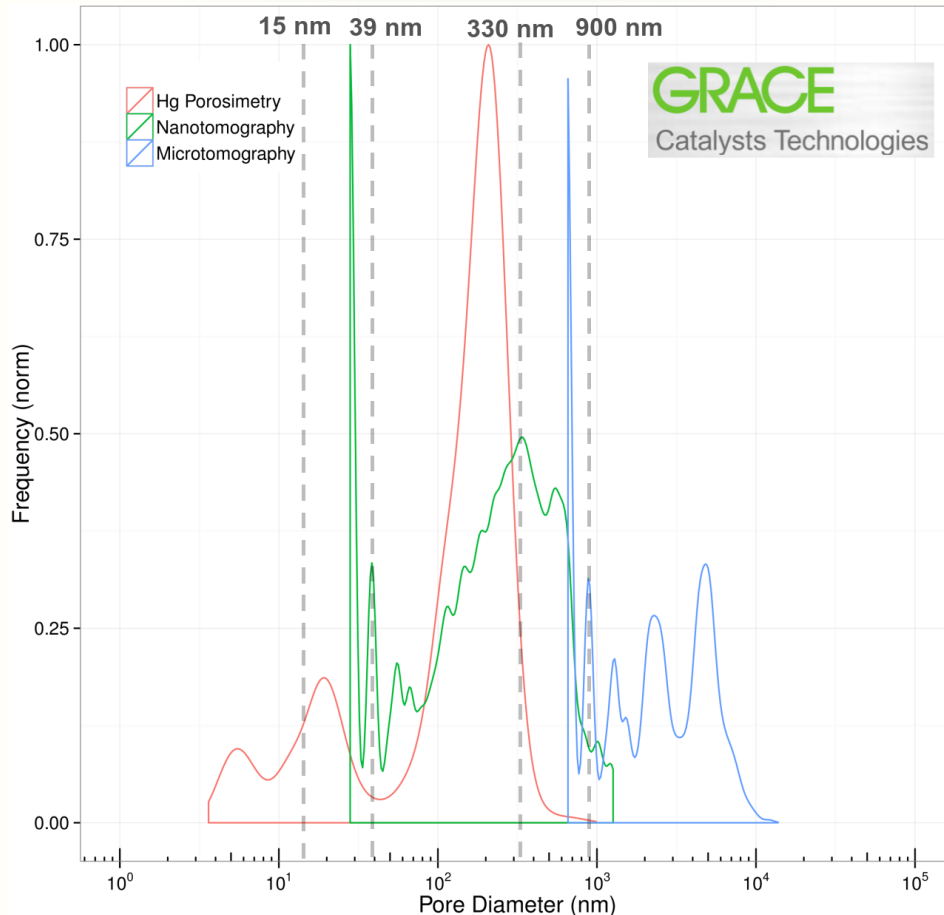


E = 6.2 keV
Resolution ≈ 39 nm
Voxel = 14 nm



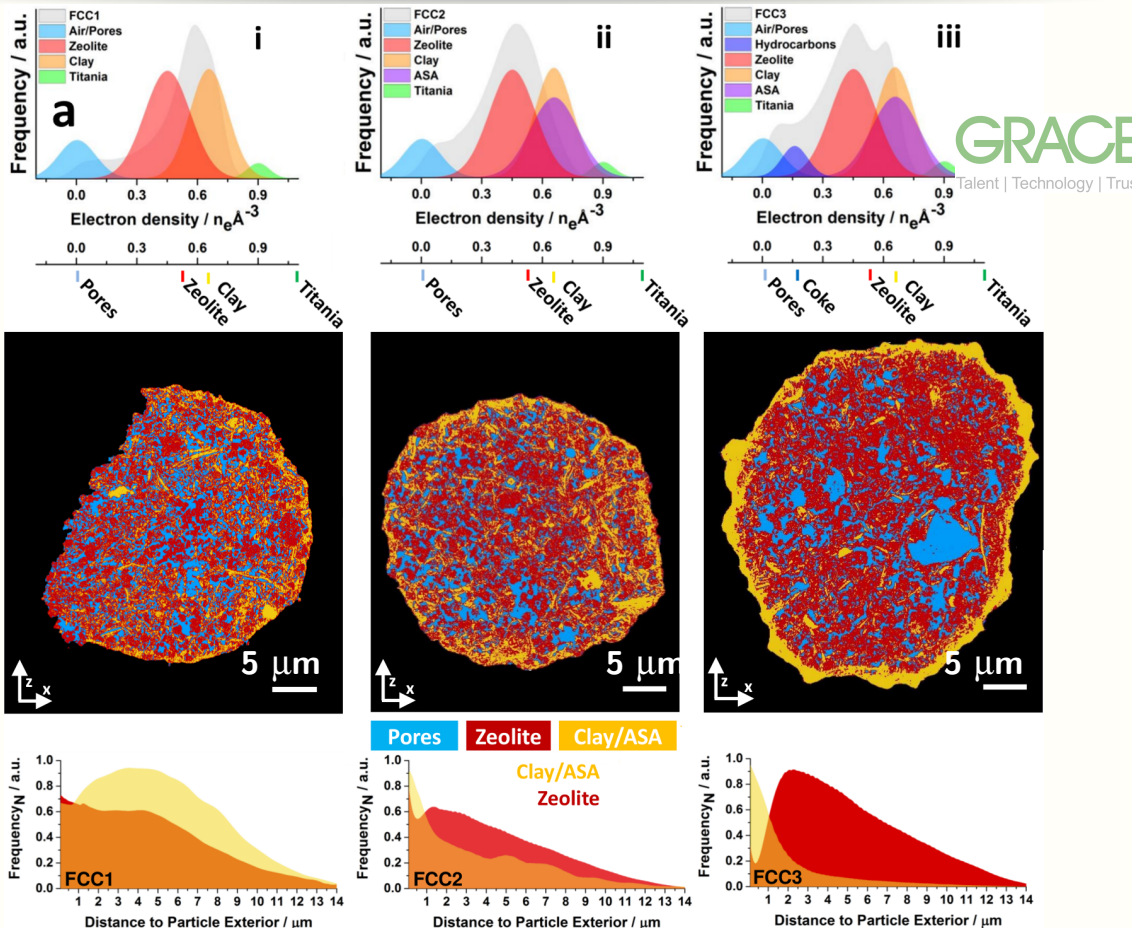
J. Ihli,..., J.C. da Silva et al., *Nature Communications* 8, 809 (2017).
J. C. da Silva et al., *ChemCatChem* 7, 413 (2015).

Pore Size Distribution from the 3D images



J. C. da Silva et al., ChemCatChem 7, (2015), 413.

Composition and morphological analysis



J. Ihli,..., J.C. da Silva et al., *Nature Communications* 8, 809 (2017).

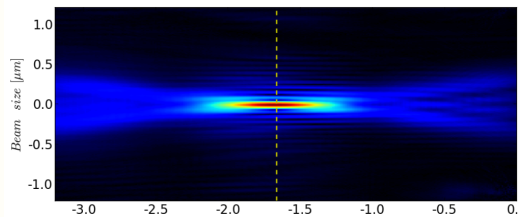
Fresnel Propagation (Angular Spectrum):

$$U_2(x, y) = \mathcal{F}^{-1} \{ \mathcal{F} \{ U_1(x, y) \} H(f_X, f_Y) \}$$

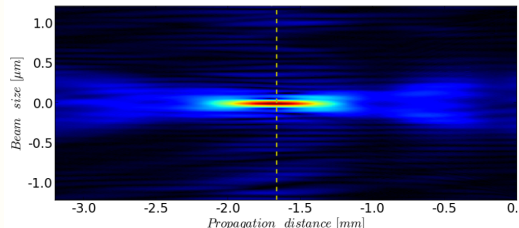
$$\text{where } H(f_X, f_Y) = \exp \left(ikz \sqrt{1 - (\lambda f_X)^2 - (\lambda f_Y)^2} \right)$$

J. Goodman, Fourier Optics (book)

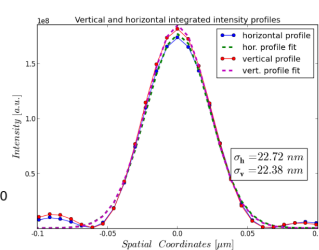
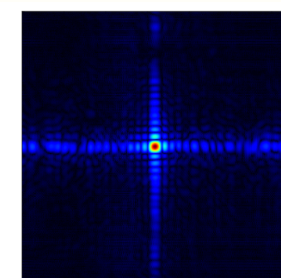
Vertical cross-section



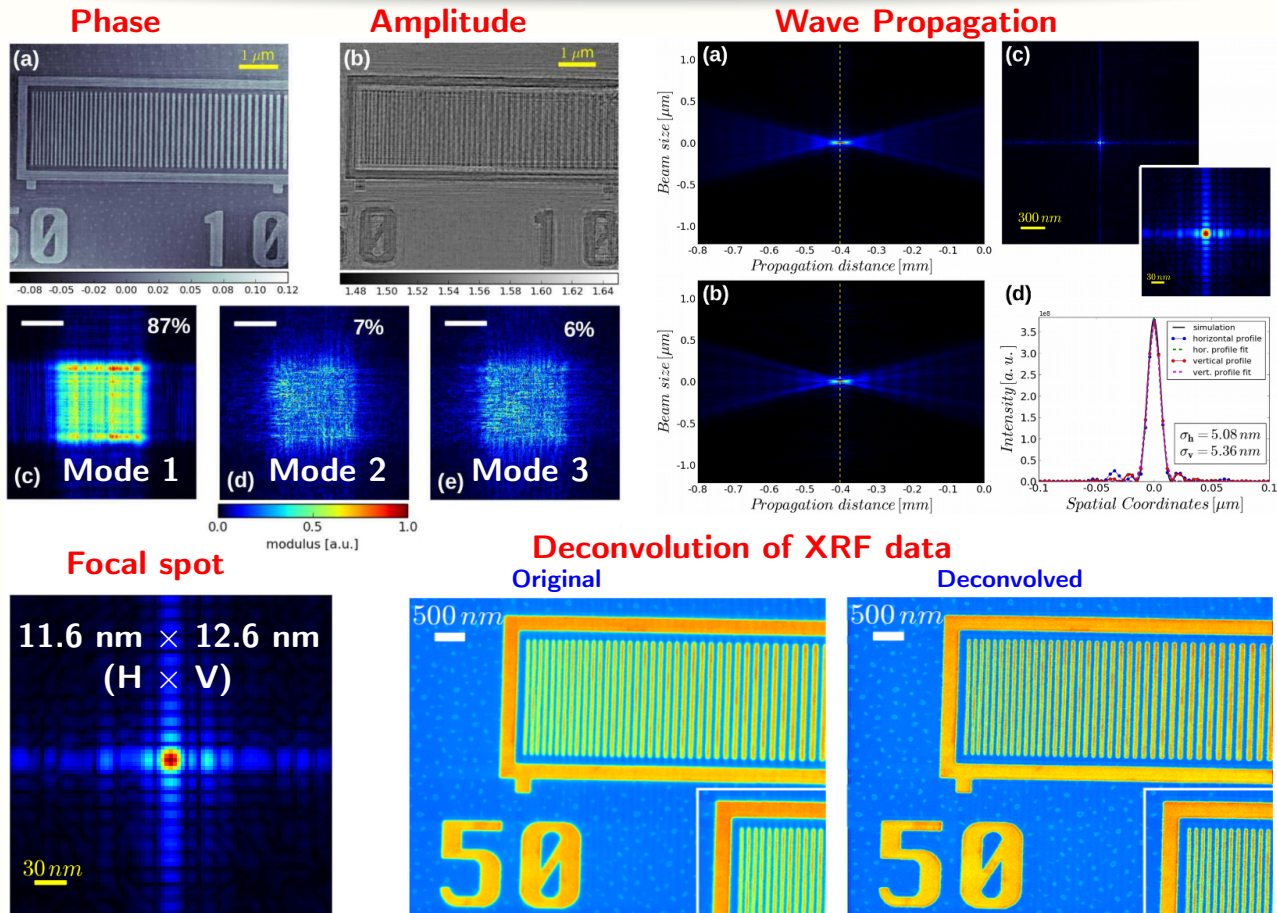
Horizontal cross-section



Beam at the focus

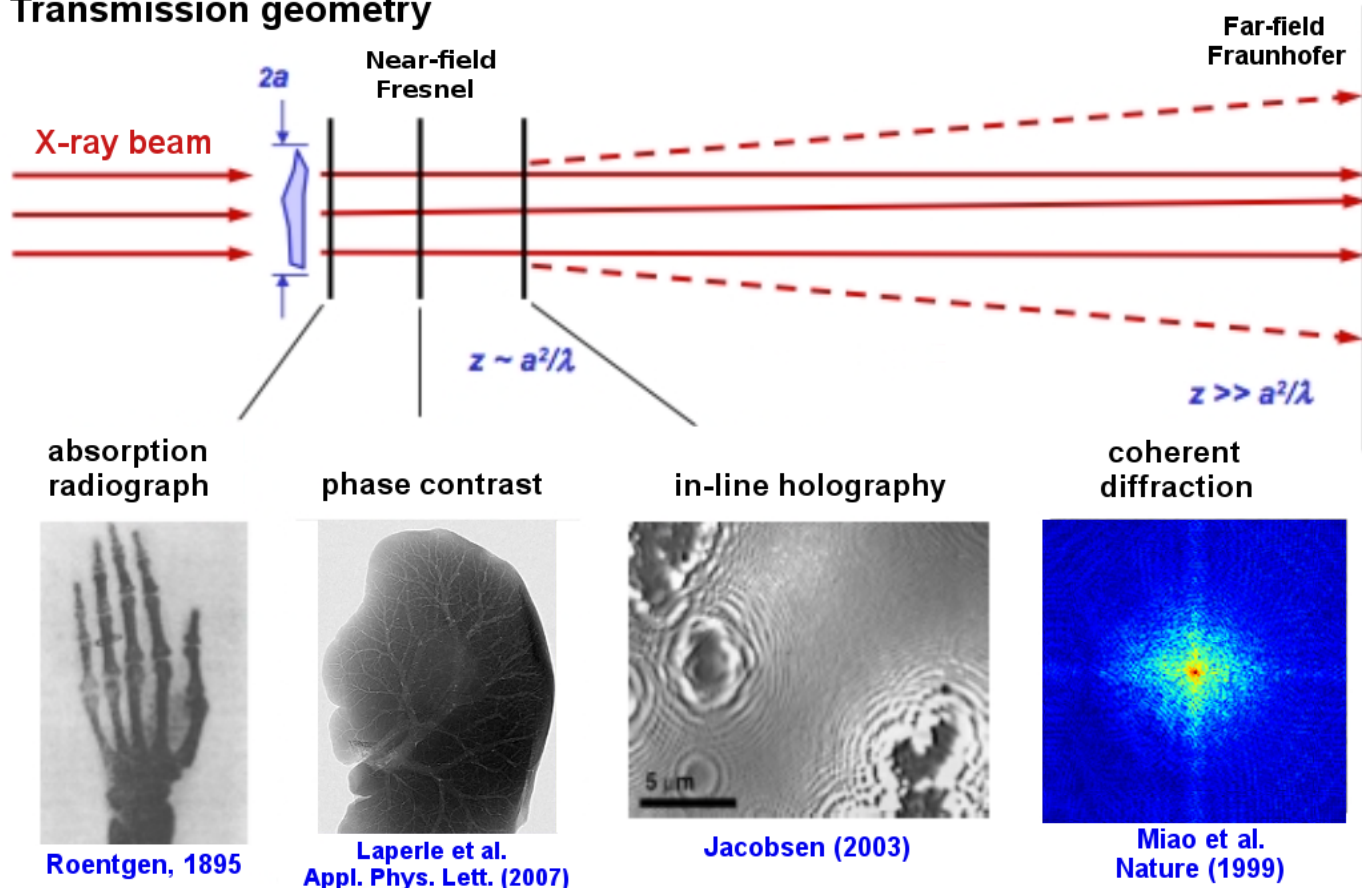


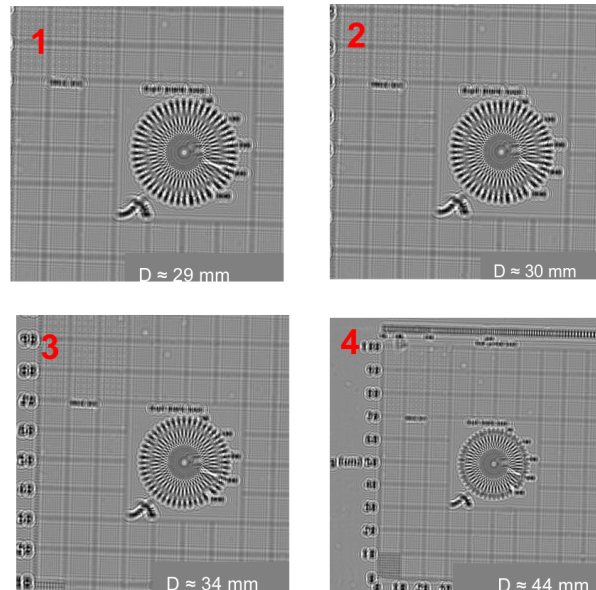
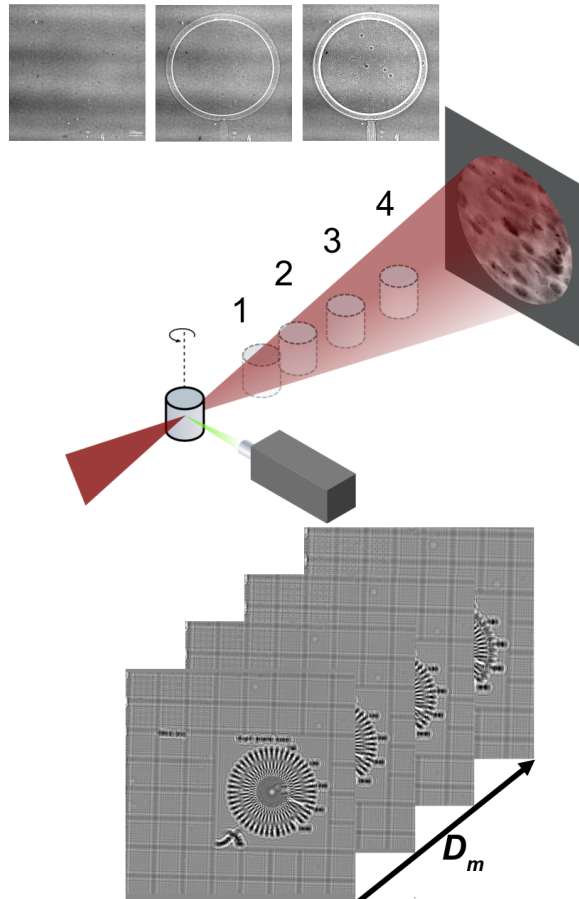
FWHM:
 $H : 64 \text{ nm}$
 $V : 63 \text{ nm}$



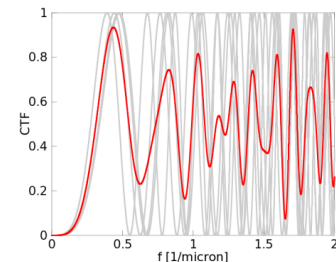
J. C. da Silva et al., Optica 4(5), 492-495 (2017).

Transmission geometry

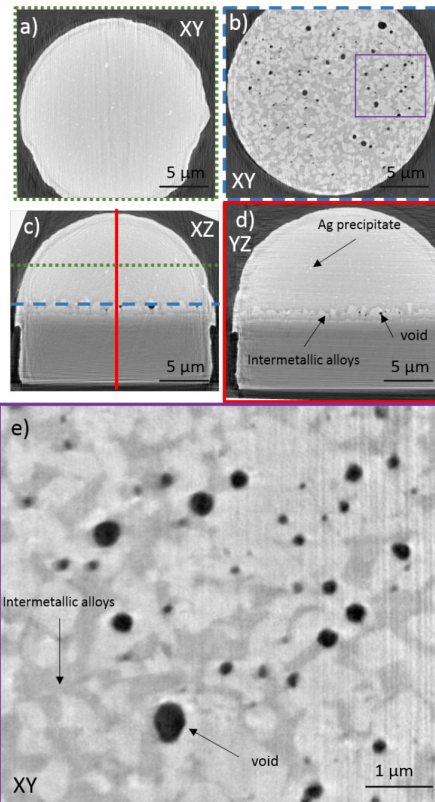
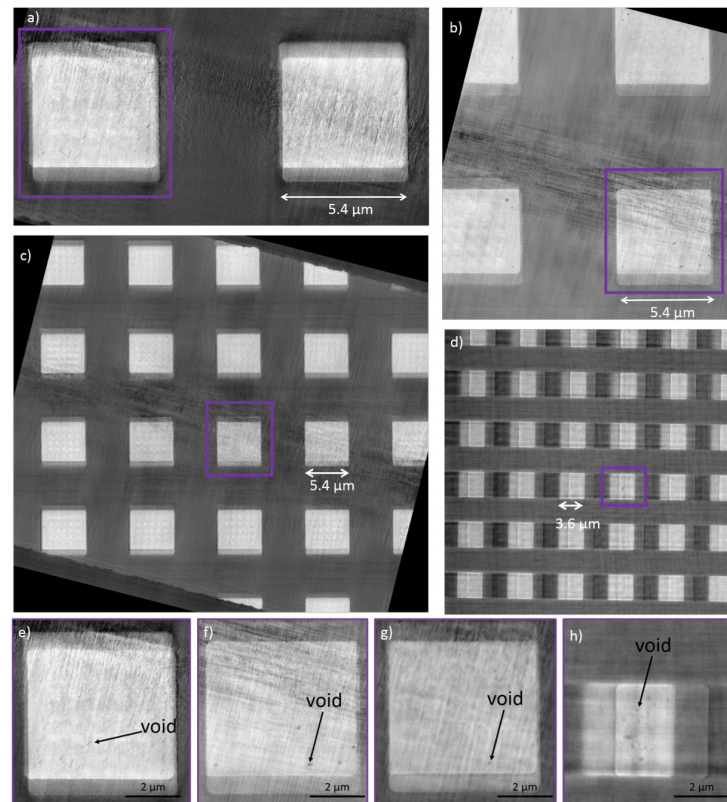




Contrast
Transfer
Function
(CTF)

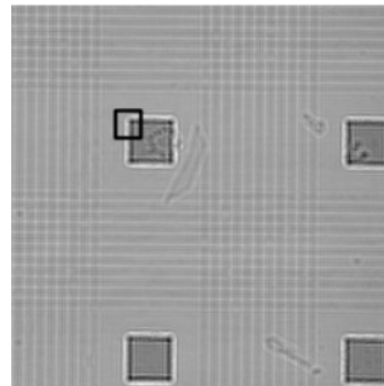


P. Cloetens et al., Appl. Phys. Lett. 75, (1999), 2912.

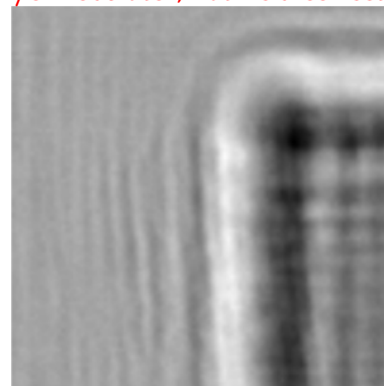
Copper pillars**Copper pads for hybrid bonding**

A. Fraczkiewicz et al., Ultramicroscopy 193, 71-83 (2018).

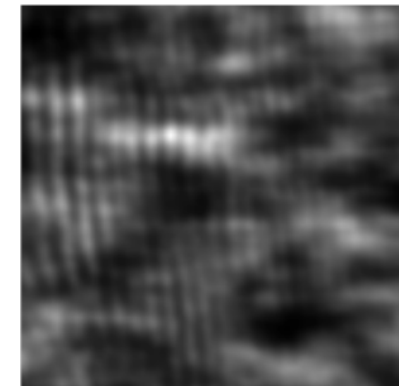
Image without modulator
After flat-field correction



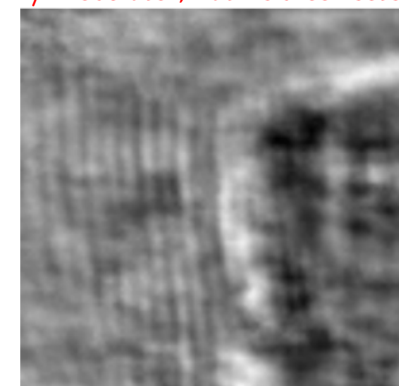
Zoomed-in region
w/o modulator, flat-field corrected

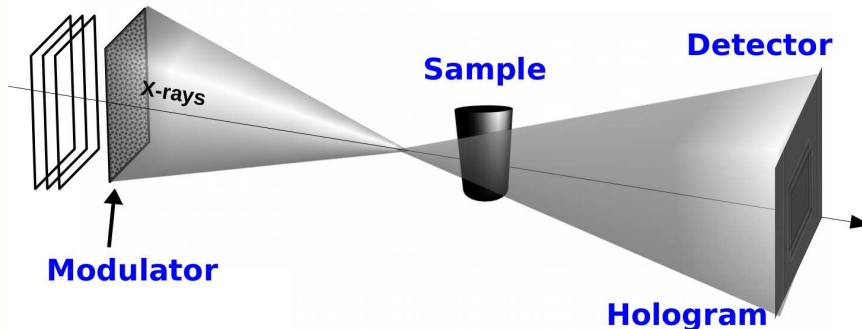
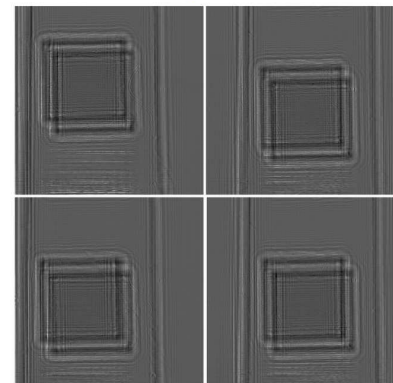
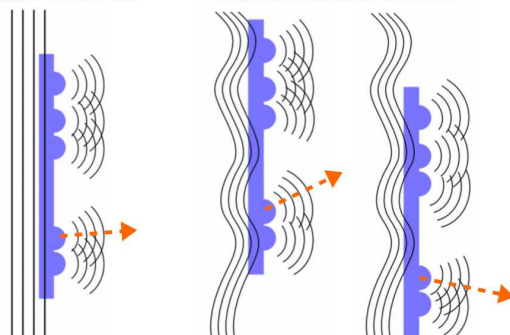
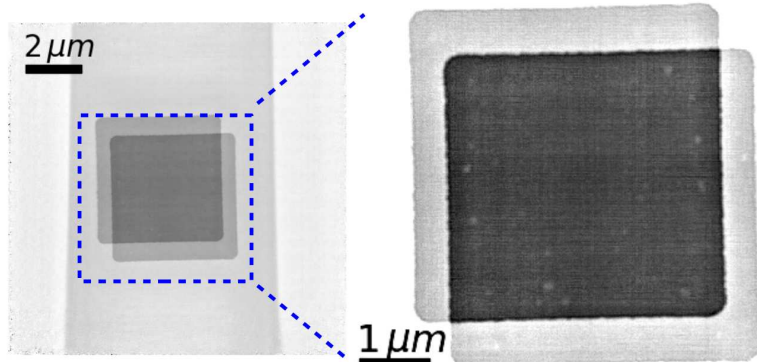


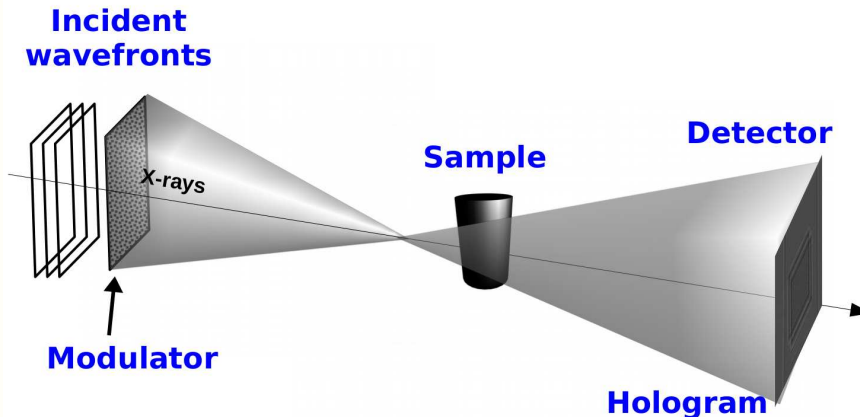
Zoomed-in region
with modulator



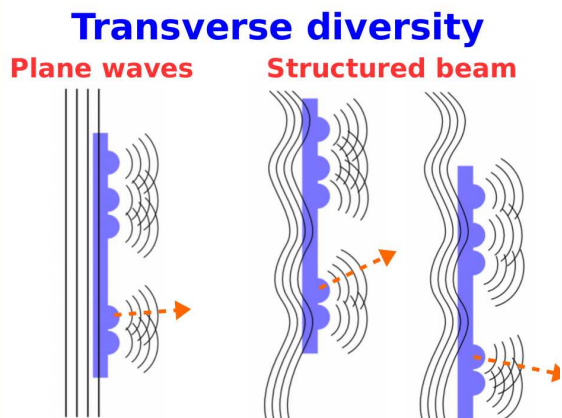
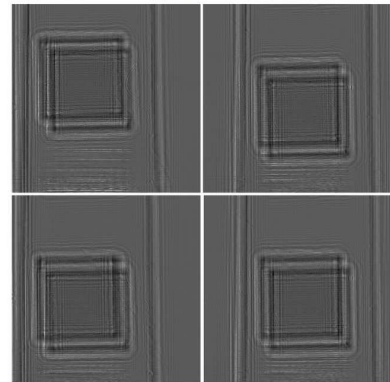
Zoomed-in region
w/ modulator, flat-field corrected



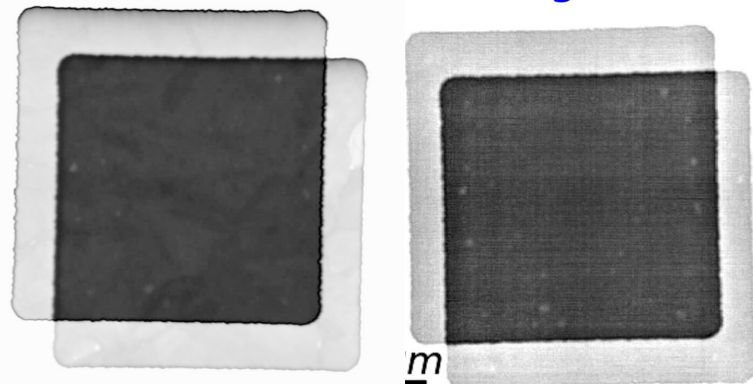
Incident wavefronts**Lateral positions****Transverse diversity****Plane waves** **Structured beam****Position R Position R+1****Reconstructed image**



Lateral positions

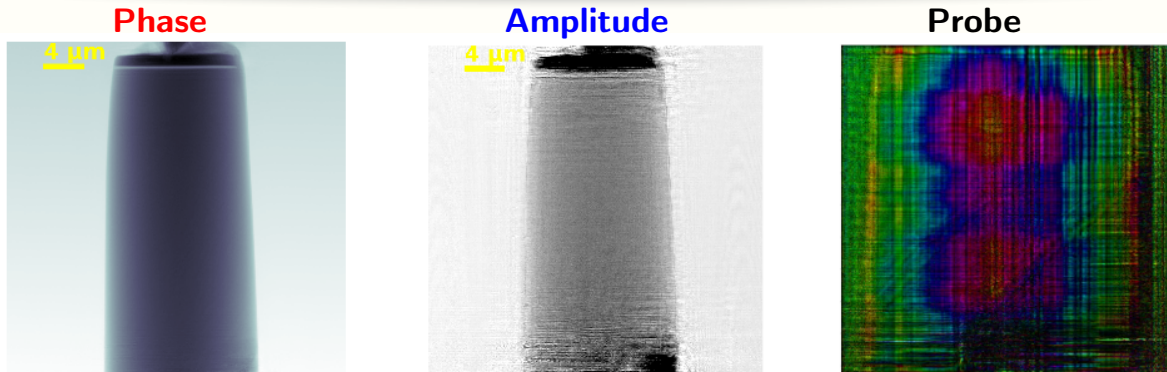


Reconstructed image



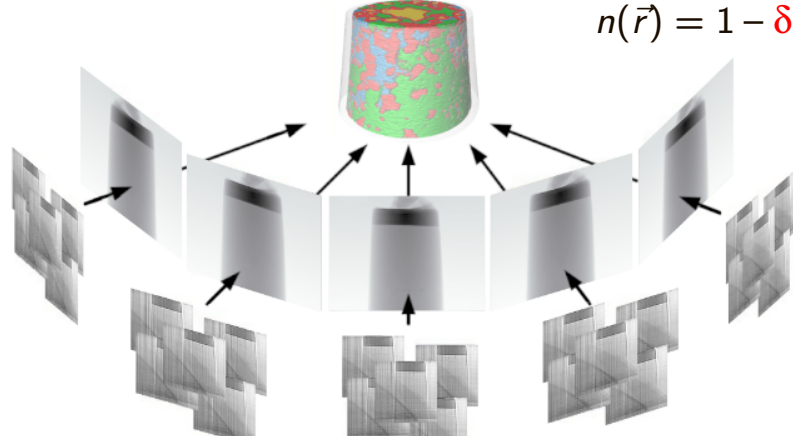
STEM

M. Stockmar et al., Sci. Rep. 3, 1927 (2013)



Near-field Ptychographic X-ray Computed Tomography (NFPXCT)

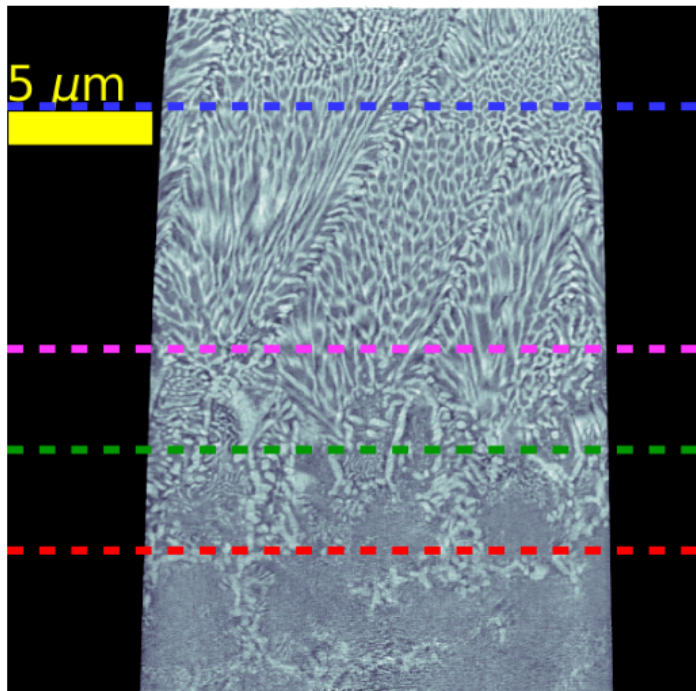
Complex-valued refractive index
 $n(\vec{r}) = 1 - \delta(\vec{r}) + i\beta(\vec{r})$



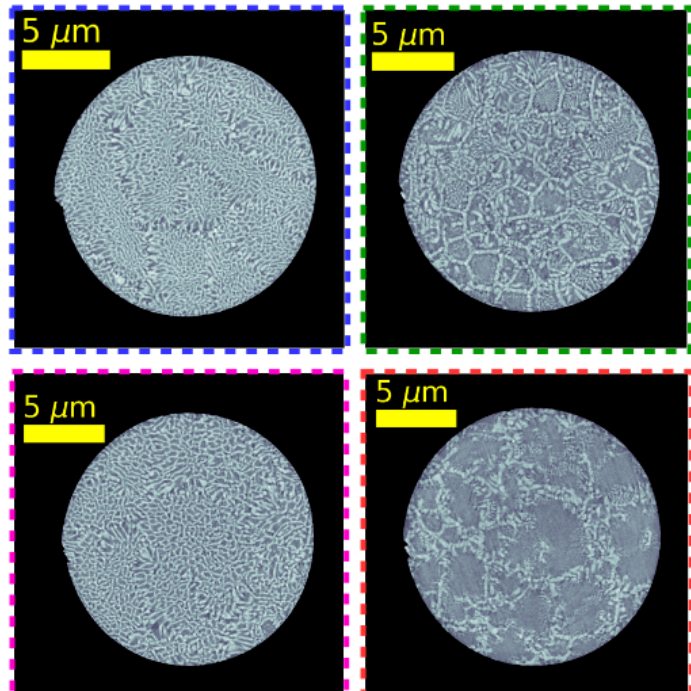
J. Gussone et al., Appl. Mat. Today 20, 100767 (2020)

M. Stockmar et al. Opt. Express 23, 12720 (2015)

Transverse slice of 3D images



Axial slices at different heights

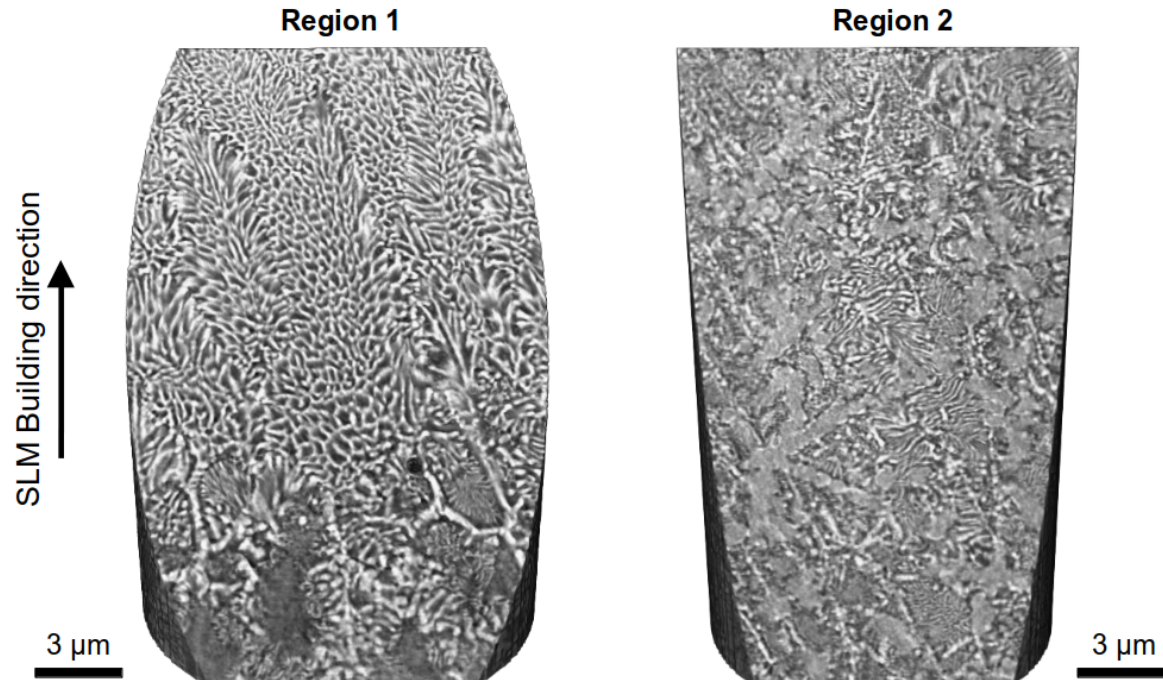


Pixel size = 15 nm and spatial resolution \approx 36 nm

J. Gussone et al., Appl. Mat. Today 20, 100767 (2020)



Deutsches Zentrum
für Luft- und Raumfahrt
German Aerospace Center



J. Gussone et al., Appl. Mat. Today 20, 100767 (2020)



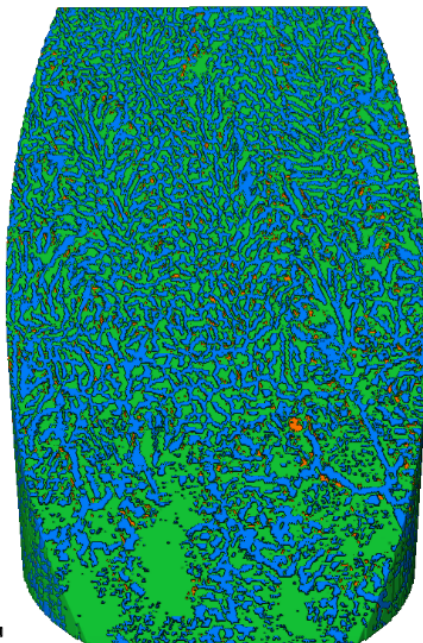
Deutsches Zentrum
für Luft- und Raumfahrt
German Aerospace Center

$\beta\text{-Ti} = 57 \text{ vol\%}$ $\text{TiFe} = 41 \text{ vol\%}$ $\alpha\text{-Ti} = 2 \text{ vol\%}$ $\text{Ti}_4\text{Fe}_2\text{O}_{0.4} = 16 \text{ vol\%}$

Region 1

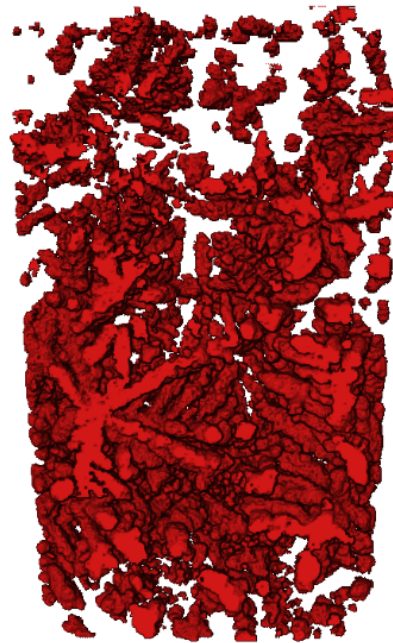
SLM Building direction

3 μm



Region 2

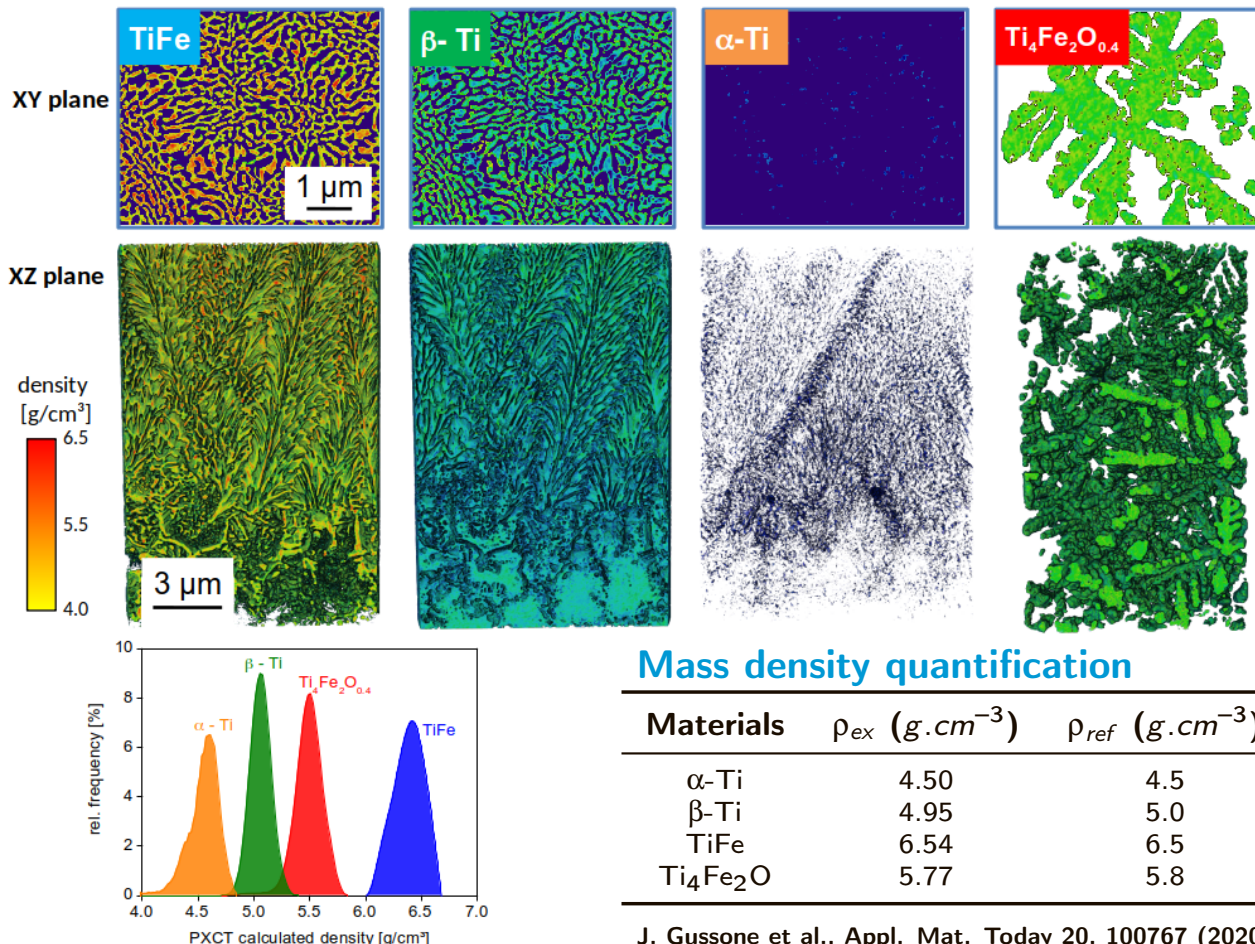
3 μm



J. Gussone et al., Appl. Mat. Today 20, 100767 (2020)

Deutsches Zentrum
für Luft- und Raumfahrt
German Aerospace Center

Analysis of the Fe-Ti alloys



Coherent X-ray imaging (2D and 3D CDI)

- High resolution, small samples, isolated specimens, works with perfect plane waves.

Far-field ptychography (FFP) & ff-PXCT

- High resolution, quantitative nanoimaging, 3D via tomography, works with plane waves or structured wavefield.

In-line holography & HXCT

- Large field-of-view, high resolution, high penetration, tomography, faster than NFP, works with perfect plane waves.

Near-field ptychography (NFP) & nf-PXCT

- Large field-of-view, relatively high resolution, quantitative nanoimaging, 3D via tomography, faster than FFP, works with structured wavefields.

Ptychographic phase retrieval



Documentation : ptycho.github.io/ptypy/
Code : <https://github.com/ptycho/ptypy>

Tomographic processing and reconstruction



Documentation : toupy.readthedocs.io
Code : github.com/jcesardasilva/toupy

2D and 3D Image processing and post-processing



NumPy
numpy.org



scipy.org



Documentation : scikit-image.org
Code : [github.com/scikit-image](https://github.com/scikit-image/scikit-image)



Documentation : porespy.readthedocs.io
Code : github.com/PMEAL/porespy

Data Visualization



matplotlib.org



github.com/enthought/mayavi



napari.org

Artificial intelligence



Documentation : tensorflow.org
Code : [github.com/tensorflow](https://github.com/tensorflow/tensorflow)



Documentation : keras.io
Code : github.com/keras-team/keras

Acknowledgements

PAUL SCHERRER INSTITUT



cSAXS group



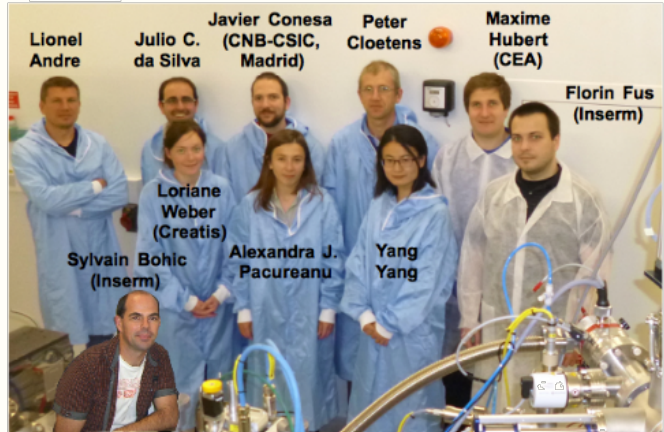
M. Holler



O. Bunk



ID16A Nano-imaging group



P. Thibault



B. Enders



G. Chahine
G. Beutier
F. Livet



M. Aranda



N. Blanc
N. Boudet
P. Bordet
J.-L. Hazemann
O. Proux



Deutsches Zentrum
für Luft- und Raumfahrt
German Aerospace Center

G. Requena
J. Haubrich
J. Gussone
P. Barriero-Vila
K. Bugelnig



J. van Bokhoven



W.-C. Cheng
Y. Shu



T. Weber

Thank you for your attention!

Contact info:

julio-cesar.da-silva@neel.cnrs.fr

Website:

sites.google.com/view/jcesardasilva

Data analysis tools:

<https://github.com/jcesardasilva>

Flash me for
more info ▼

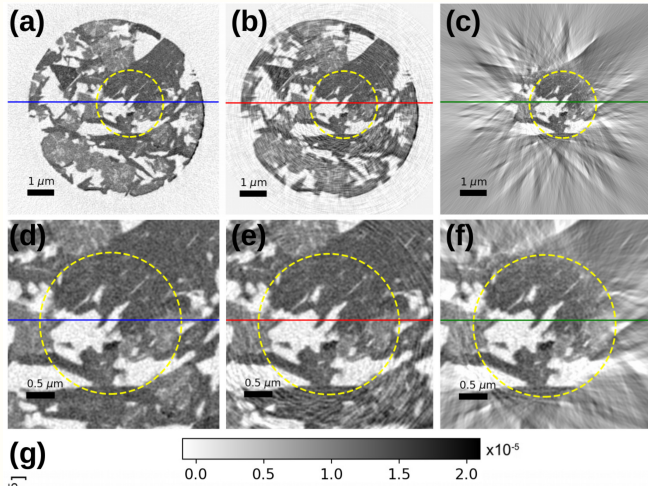


QR code

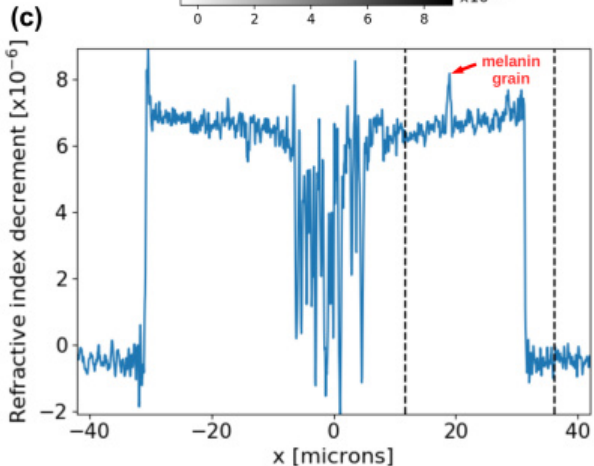
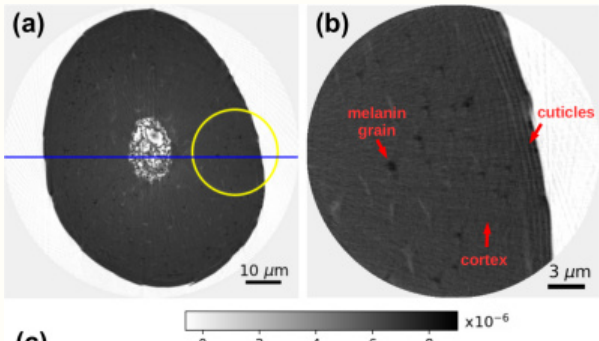
Extra slides

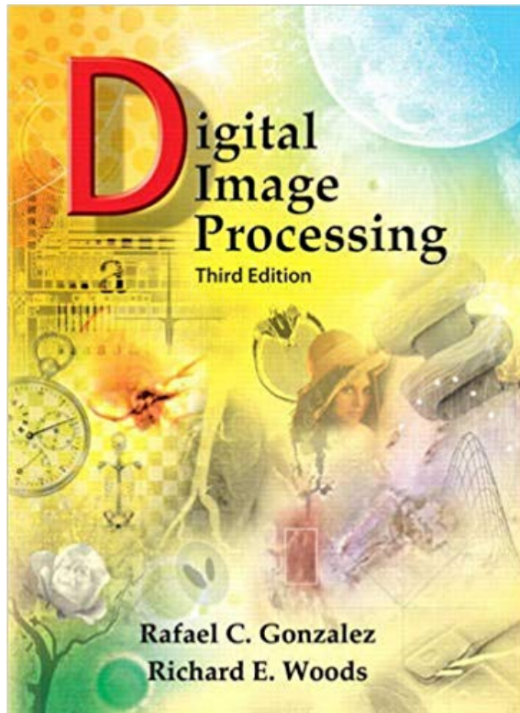
Region-of-interest tomography PXCT in local tomography mode

FCC catalyst body



Human hair





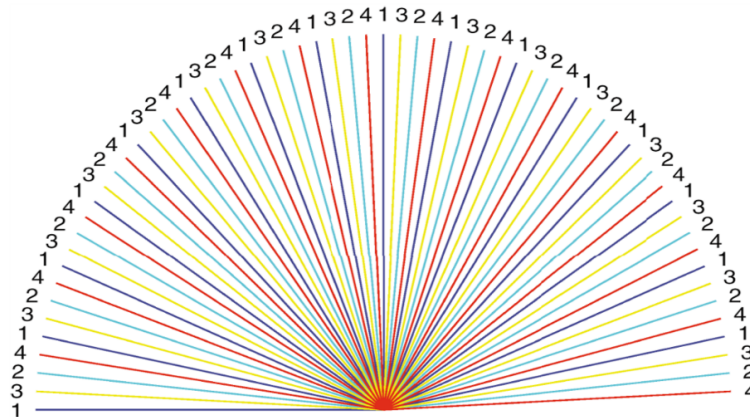
2.4.3 Spatial and Intensity Resolution

Intuitively, spatial resolution is a measure of the smallest discernible detail in an image. Quantitatively, *spatial resolution* can be stated in a number of ways, with *line pairs per unit distance*, and *dots (pixels) per unit distance* being among the most common measures. Suppose that we construct a chart with alternating black and white vertical lines, each of width W units (W can be less than 1). The width of a *line pair* is thus $2W$, and there are $1/2W$ line pairs per unit distance. For example, if the width of a line is 0.1 mm, there are 5 line pairs per unit distance (mm). A widely used definition of image resolution is the largest number of *discernible* line pairs per unit distance (e.g., 100 line pairs per mm). Dots per unit distance is a measure of image resolution used commonly in the printing and publishing industry. In the U.S., this measure usually is expressed as *dots per inch* (dpi). To give you an idea of quality, newspapers are printed with a resolution of 75 dpi, magazines at 133 dpi, glossy brochures at 175 dpi, and the book page at which you are presently looking is printed at 2400 dpi.

The key point in the preceding paragraph is that, to be meaningful, measures of spatial resolution must be stated with respect to spatial units. Image size by itself does not tell the complete story. To say that an image has, say, a resolution 1024×1024 pixels is not a meaningful statement without stating the spatial dimensions encompassed by the image. Size by itself is helpful only in making comparisons between imaging capabilities. For example, a digital camera with a 20-megapixel CCD imaging chip can be expected to have a higher capability to resolve detail than an 8-megapixel camera, assuming that both cameras are equipped with comparable lenses and the comparison images are taken at the same distance.

Intensity resolution similarly refers to the smallest discernible change in intensity level. We have considerable discretion regarding the number of samples used to generate a digital image, but this is not true regarding the number

Binary acquisition:



Number of
projections:

$$N = \frac{\pi}{2} \left(\frac{a}{\Delta r} \right)$$

F. Natterer, *The Mathematics of Computerized Tomography* (book)

A. C. Kak and M. Slaney, *The principals of computerized tomographic imaging* (book)

A. Kaestner et al., *Opt. Eng.* 50 (2011) 123201

M. Holler et al., *Scientific Reports* 4 (2014) 3857